

ELECTRODYNAMICS OF MAGNETARS IV:
SELF-CONSISTENT MODEL OF THE INNER ACCELERATOR
WITH IMPLICATIONS FOR PULSED RADIO EMISSION

CHRISTOPHER THOMPSON
CITA, 60 St. George St., Toronto, ON M5S 3H8, Canada
Submitted to the Astrophysical Journal

ABSTRACT

We consider the voltage structure in the open-field circuit and outer magnetosphere of a magnetar. The standard polar-cap model for radio pulsars is modified significantly when the polar magnetic field exceeds 1.8×10^{14} G. Pairs are created by accelerated particles via resonant scattering of thermal X-rays, followed by the nearly instantaneous conversion of the scattered photon to a pair. A surface gap is then efficiently screened by e^{\pm} creation, which regulates the voltage in the inner part of the circuit to $\lesssim 10^9$ V. We also examine the electrostatic gap structure that can form when the magnetic field is somewhat weaker, and deduce a voltage 10–30 times larger over a range of surface temperatures. We examine carefully how the flow of charge back to the star above the gap depends on the magnitude of the current that is extracted from the surface of the star, on the curvature of the magnetic field lines, and on resonant drag. The rates of different channels of pair creation are determined self-consistently, including the non-resonant scattering of X-rays, and collisions between gamma rays and X-rays. We find that the electrostatic gap solution has too small a voltage to sustain the observed pulsed radio output of magnetars unless i) the magnetic axis is nearly aligned with the rotation axis and the light of sight; or ii) the gap is present on the closed as well as the open magnetic field lines. Several properties of the radio magnetars – their rapid variability, broad pulses, and unusually hard radio spectra – are consistent with a third possibility, that the current in the outer magnetosphere is strongly variable, and a very high rate of pair creation is sustained by a turbulent cascade.

Subject headings: plasmas — radiation mechanisms: non-thermal — stars: magnetic fields, neutron

1. INTRODUCTION

Magnetars are persistent sources of broad band, non-thermal radiation (see Woods & Thompson 2006 for a recent review). The discovery of pulsed radio emission from XTE J1810–197 and 1E 1547.0–5408 (Halpern et al. 2005; Camilo et al. 2006, 2007a,b) adds to the body of evidence identifying them as isolated, non-accreting neutron stars. This radio emission is peculiar in several respects: its brightness fluctuates strongly on a timescale of minutes to days, and peaks above a frequency of 100 GHz. The detection of pulsed radio emission from two magnetars, some 15 percent of the presently known population, appears to be a consequence of the surprisingly large pulse duty cycle. The known magnetars spin with typical periods of several seconds, and their open field lines form a narrow bundle close to the star. For this reason, it had generally been expected that their radio emission would be strongly beamed.

The output of a magnetar in the hard X-ray band can greatly exceed the spindown power of the star (Kuiper et al. 2004, 2006), and so most of the underlying dissipation is probably concentrated in the closed magnetosphere (Thompson & Beloborodov 2005; Baring & Harding 2007). The same energetic argument does not apply to the radio output, which is smaller than the spindown luminosity. The radio emission zone could, therefore, be restricted to the open magnetic field lines.

It has also been suggested that relatively strong currents flow within the outer magnetosphere of a magnetar, being sustained by the outward transfer of twist from an inner zone where it is injected by starquakes. This redistribution of the twist causes the poloidal field lines to expand slightly, thereby increasing the open-field voltage (Thompson et al. 2002). The effect depends on the extraction of a tiny fraction the helicity that is stored in the inner magnetosphere and stellar interior. The radio brightness of the magnetar XTE J1810–197 is observed to correlate strongly with the spindown torque (Camilo et al. 2007a), a behavior which is consistent with this type of structural change. Indeed, the torque variations measured in XTE J1810–197 are comparable in magnitude to those seen in the Soft Gamma Repeaters, which are much more variable in the X-ray band (Woods et al. 2002).

The injection of twist into the outer magnetosphere inevitably triggers current-driven instabilities and strong fluctuations in the current. A detailed model of pair creation in a dynamic open magnetic flux tube is given in a companion paper (Thompson 2008; see also Lyutikov & Thompson 2008). The torsional oscillations of the magnetic field cascade to high frequencies if their amplitude exceeds a critical value, resulting in a very high rate of pair creation.

In this paper, focus on the case where the current that is drawn from the magnetar surface varies only slowly on the timescale R_{NS}/c , where R_{NS} is the stellar radius. Our main goal is to work out the structure of a pair-creating diode forming at the surface when the magnetic field is stronger than the QED value $B_{\text{Q}} = 4.4 \times 10^{13}$ G. The voltage across the diode is influenced by several competing effects: the mechanism(s) of pair creation; the charge flow in the outer magnetosphere; and the gradient in the corotation charge density ρ_{GJ} at the stellar surface. Our solution applies, in principle, to both the open and the extended closed magnetic field lines, because it depends only on the flux of charges returning from the outer magnetosphere.

A detailed review of the basic QED processes leading to pair creation in super-QED magnetic fields is given in Usov & Melrose (1996), and a companion paper (Thompson 2008). The dominant mechanism of pair creation involves the creation of gamma

rays by resonant scattering of thermal X-rays (Kardashev et al. 1984, Daugherty & Harding 1989, Sturmer 1995, and Hibschan & Arons 2001a,b). The voltage across a gap can also be regulated by collisions between gamma rays and thermal X-rays (e.g. Zhang & Qiao 1998) and, as we show in this paper, by the direct conversion of non-resonantly scattered X-rays to pairs.

One of our main results is that a diode *cannot* be self-consistently be maintained at the surface when the magnetic field $B_{\text{NS}} > 4B_{\text{Q}} = 1.8 \times 10^{14}$ G. In this case, the scattered photon is typically above threshold for pair creation, and there is essentially no delay between the creation of a gamma ray and its conversion to a pair (Beloborodov & Thompson 2007). We describe a circuit solution that has an inward e^{\pm} discharge, within which the voltage that is screened to a low value $\lesssim 10^9$ V. The stability of this solution is also investigated, and is shown explicitly to depend on a delay between gamma-ray emission and pair creation.

A surface gap is possible when $B_{\text{NS}} < 4B_{\text{Q}}$ and the current density is larger than $\rho_{\text{GJ}}c$. We construct a detailed model including all the relevant modes of pair creation. We focus on space-charge limited flows, and explain why charges of both signs can be supplied continuously from the surface of a magnetar. Even through heavy atoms are tightly bound into molecular chains (Medin & Lai 2007, and references therein), ions can be liberated from the magnetar surface by photoionization and knockout processes.

The equilibrium gap voltage is calculated as a function of the X-ray black body temperature T_{bb} of the stellar surface. It is gradually reduced as $k_{\text{B}}T_{\text{bb}}$ rises above $\sim 0.15 - 0.2$ keV, and non-resonant scattering and photon collisions supply increasing amounts of pair creation within the gap. Pairs that are created just outside the gap continue to lose energy by resonant scattering, and the resulting increase in the pair multiplicity is derived. We explain in detail how the polarization of a pair-creating cloud that is formed just outside the diode will create enough returning charges to compensate the gradient in corotation charge density outside the gap.

An important subtlety involves the effect of cyclotron drag at ~ 10 stellar radii; we show that outside this zone the correct space charge is obtained if the charges of sign opposite to ρ_{GJ} flow outward sub-relativistically. This solution breaks down beyond a critical angle from the magnetic axis, where charges of both signs can be decelerated to trans-relativistic speeds. As a result, we point out that there is a selection effect against observing pulsed radio emission from X-ray bright neutron stars with spin periods shorter than ~ 0.3 seconds. The reflection of gamma rays back toward the star via resonant scattering can have a similar effect at much longer spin periods.

The plan of the paper is as follows. The origin of the open-field voltage is reviewed in § 2, and the two basic types of circuit solution – with and without a diode – are described. The voltage of a surface diode in a magnetic field $\lesssim 4B_{\text{Q}}$ is derived in §3, and the effects of cyclotron drag are investigated in §4. In section 5 we explore in detail the plasma flow on the open field lines when $B_{\text{NS}} > 4B_{\text{Q}}$ and a diode is absent at the surface of the star. The paper closes with a summary of how the different circuit solutions described in the paper are constrained by the luminosities of the radio magnetars. The Appendix compares the effects of field-line bending and general-relativistic frame dragging on the gradient in corotation charge density.

2. VOLTAGE GENERATION

In the absence of pair creation, a very large voltage develops on the open magnetic field lines of a rotating neutron star. When the effects of screening by pair creation are included, the magnitude and time dependence of the voltage are believed to depend on several factors (e.g. Sturrock 1971; Ruderman & Sutherland 1975; Scharlemann, Arons, & Fawley 1978). A vacuum gap could form with a relatively large and variable voltage when the corotation charge density is positive, if the ions are tightly bound in molecular chains to the neutron star surface. Although magnetars are indeed expected to have condensed surfaces in the absence of a hydrogen or helium layer (Medin & Lai 2007), it is plausible that photodissociation and spallation process will liberate ions at a sufficient rate to supply the spindown current (Section 2.3). We therefore assume a continuous charge flow from the magnetar surface, for either sign of ρ_{GJ} .

The voltage that develops in this case has generally been thought to be regulated by the gradient in ρ_{GJ} away from the neutron star surface. The dominant contributions to this gradient come from general relativistic frame dragging (Muslimov & Tsygan 1992) and magnetic field line curvature (Scharlemann et al. 1978). The second effect may well be dominant in magnetars, given the strong evidence for a non-dipolar field structure in the light curves of SGR flares (Thompson & Duncan 2001).

The main assumption here is that the current that is drawn from the neutron star surface can be supplied very nearly by a flow of outgoing and returning charges,

$$J \simeq \rho_{\triangleright}v_{\triangleright} + \rho_{\triangleleft}v_{\triangleleft} \simeq (\rho_{\triangleright} - \rho_{\triangleleft})c. \quad (1)$$

In our basic one-dimensional model, the current density J is nearly aligned with the background magnetic field, and ρ_{\triangleright} and ρ_{\triangleleft} are the densities of outgoing and ingoing charges. The flux of ingoing charges is provided by pair creation within the circuit.

We consider two basic circuit solutions. In the first case, the pair creation is distributed smoothly throughout the circuit, so as to maintain the local charge balance

$$\rho_{\triangleright}(z) + \rho_{\triangleleft}(z) = \rho_{\text{GJ}}(z). \quad (2)$$

Here ρ_{GJ} is the corotation charge density. The second basic type of circuit solution involves a plasma-filled gap of height h , which sits at the base of the circuit. Charges moving outward through this gap gain enough energy to emit gamma rays that are able to convert to pairs at $z > h$, thereby creating a dense polarizable plasma. The gap voltage can also be limited by pair creation by ingoing charges, and by modes of pair creation that are distributed throughout the volume of the gap (§3).

In a Newtonian gravitational field, the corotation charge density would be given by (Goldreich & Julian 1969)

$$\rho_{\text{GJ}}^0 = -\frac{1}{4\pi c} \nabla \cdot (\mathbf{v} \times \mathbf{B}) = -\frac{\boldsymbol{\Omega} \cdot \mathbf{B}}{2\pi c}. \quad (3)$$

This result is modified by relativistic effects: in particular, the rotation of the neutron star drags the frame of a zero angular-

momentum observer with an angular velocity $\omega = \kappa\Omega$, where the coefficient is given by¹

$$\kappa(r) = \kappa_{\text{NS}} \left(\frac{r}{R_{\text{NS}}} \right)^{-3}, \quad \kappa_{\text{NS}} = \frac{2GI_{\text{NS}}}{R_{\text{NS}}^3 c^2} = 0.15 I_{\text{NS},45} R_{\text{NS},6}^{-3}. \quad (4)$$

Here I_{NS} is the moment of inertia of the neutron star, and R_{NS} its radius. This has the effect of reducing the corotation charge density,²

$$\rho_{\text{GJ}} = \rho_{\text{GJ}}^0 [1 - \kappa(r)]. \quad (5)$$

The normalized charge density ρ_{GJ}/B increases with radius along a straight magnetic field line.

If the higher order multipole components of the magnetic field are comparable in strength to the dipole near the neutron star surface, then a stronger voltage can be produced than purely by the frame dragging effect (Barnard & Arons 1982; Asseo & Khechinashvili 2002). As we show in Appendix A, the leading contribution to the field line curvature comes from the octopole component of the magnetic field, and the quadrupole component to second order, when these two components are treated as a perturbation to the dipole,

$$B \frac{d(\rho_{\text{GJ}}/B)}{dl} = \frac{\rho_{\text{GJ}}}{R_C} \sin \chi \cos \phi_C = \tilde{\kappa}_3 \frac{\rho_{\text{GJ}}}{R_{\text{NS}}} \left(\frac{r}{R_{\text{NS}}} \right)^{-3}. \quad (6)$$

Here R_C is the curvature radius and the coefficient $\tilde{\kappa}_3$ is expressed in terms of the surface amplitudes $\varepsilon_{2,3}$ of the quadrupole and octopole via

$$\tilde{\kappa}_3 = \left(\varepsilon_3 + \varepsilon_2 \frac{\partial \varepsilon_2}{\partial \theta} \right) \sin \chi \cos \phi_C. \quad (7)$$

In addition, χ is the angle between the magnetic moment μ and the rotation axis Ω , and ϕ_C the angle between the plane of curvature of the magnetic field lines and the $\mu - \Omega$ plane.

A subtlety associated with this model, which has not been fully explored, is that the value of J that is demanded by the outer magnetosphere need not closely match an outward charge flow of density ρ_{GJ} and speed c . When the current density is smaller in magnitude than $\rho_{\text{GJ}}c$ and has the same sign, the open-field voltage remains modest close to the star,³ and the mean flow speed of the outgoing charges is smaller than the speed of light (Mestel et al. 1995; Shibata 1997; Beloborodov 2007). We therefore focus here on the case where J is larger in magnitude than $\rho_{\text{GJ}}c$, allowing for the possibility that J may have the opposite sign. Such an imbalance could naturally result from a multipolar structure in the external magnetic field of the magnetar; and from more subtle effects such as resistive instabilities in the current carrying flux tube or more exotic effects such as the loss of magnetic helicity from the closed magnetosphere onto the open field lines.

2.1. Voltage Solution I without an Inner Gap and Pair Multiplicity ~ 1

We now describe a simple model for the inner part the open field circuit, within which pair are created at the minimum rate needed to balance the gradient in ρ_{GJ} along the magnetic field. This zone extends from the neutron star surface out to a maximum radius R_* , which is determined self-consistently by the stability of the solution (§5.1). The range of radii considered here is much broader than the width of the open-field bundle, i.e. $R_* - R_{\text{NS}} \gg R_{\text{NS}} \theta_{\text{open}}(R_{\text{NS}})$, where $\theta_{\text{open}}(r) = (\Omega r/c)^{1/2}$. The circuit can, therefore, be approximated as a thin tube.

We take the flow to be steady, with all particles moving relativistically and charges of opposite signs moving in opposite directions. Implicit in this setup is the assumption that one particle in each newly created e^\pm pair reverses direction nearly instantaneously. The flows of ingoing and outgoing charges satisfy the usual continuity equations,

$$c \frac{d}{dr} (n_{\triangleright} S_{\perp}) = \dot{n}_{\pm} S_{\perp}, \quad (8)$$

$$-c \frac{d}{dr} (n_{\triangleleft} S_{\perp}) = \dot{n}_{\pm} S_{\perp}, \quad (9)$$

where $\dot{n}_{\pm} = (\dot{n}_e + \dot{n}_{e^+})/2$ is the rate of creation of electrons and positrons per unit volume, and S_{\perp} (eq. [A16]) is the cross sectional area of the open field-line bundle at radius r . The gradient in the total charge density $\rho = \rho_{\triangleright} + \rho_{\triangleleft}$ is obtained from the sum of equations (8) and (9). One finds

$$c \frac{d}{dr} (\rho S_{\perp}) = 2e \dot{n}_{\pm} S_{\perp} \text{sgn}(\rho_{\text{GJ}}), \quad (10)$$

where e is the magnitude of the electron charge.

As is shown below, the electric field $E_{\parallel} = \mathbf{E} \cdot \hat{\mathbf{B}}$ is greatly reduced compared with the unscreened value in the absence of pair creation. The small E_{\parallel} is sustained by a small fractional departure of ρ from the local corotation charge density. Therefore,

$$\rho(r) \simeq \rho_{\text{GJ}}(r). \quad (11)$$

¹ Throughout this paper we use the shorthand $X = X_n \times 10^n$, where the value of quantity X is measured in c.g.s. units.

² The quantity on the left-hand side is, strictly, the product of the lapse function $\alpha(r)$ and the proper charge density, but this subtlety can be neglected in our present treatment because B and the current density $\alpha \rho_{\text{GJ}} v$ both satisfy the same conservation equation.

³ This statement does not apply to the outer magnetosphere, where part of the open-field bundle crosses the surface where $\Omega \cdot \mathbf{B}$ vanishes; in other words, an outer gap can still be present even in the absence of an inner gap.

Associated with this charge density is a net outward flow of particles moving at $v \simeq c$,

$$\dot{N}_{\text{GJ}} = \frac{1}{e} |\rho_{\text{GJ}}| S_{\perp} c \equiv \frac{|I_{\text{GJ}}|}{e}, \quad (12)$$

The continuity equation (10) can then be written as

$$\dot{n}_{\pm} S_{\perp} = \frac{1}{2} \frac{d\dot{N}_{\text{GJ}}}{dr}, \quad (13)$$

A specific example in which pair creation is driven by resonant scattering is described in §5.

In this toy model, the net current along the open field-line bundle is in a steady state,

$$I_{\triangleright} + I_{\triangleleft} = I = \text{const}, \quad (14)$$

where $I_{\triangleright} = c\rho_{\triangleright}S_{\perp}$ and $I_{\triangleleft} = -c\rho_{\triangleleft}S_{\perp}$. The strength of the current is determined by conditions in the outer magnetosphere, and does not influence the qualitative nature of the solution. In particular, current-driven instabilities in the outer magnetosphere are assumed to occur on timescales much longer than the light-crossing time of the inner circuit, so that changes in I occur adiabatically. (This assumption will break down if the outer magnetosphere is strongly dynamic, so that a turbulent spectrum of modes is established by non-linear couplings between the waves: Lyutikov & Thompson 2005; Thompson 2008.)

Using $\rho \simeq \rho_{\text{GJ}}$ we also have

$$I_{\triangleright} - I_{\triangleleft} = I_{\text{GJ}}. \quad (15)$$

Equations (14) and (15) imply

$$I_{\triangleleft} = \frac{1}{2} (I - I_{\text{GJ}}), \quad \frac{dI_{\triangleleft}}{dr} = -\frac{1}{2} \frac{dI_{\text{GJ}}}{dr}. \quad (16)$$

The outward current density can therefore differ significantly from I_{GJ} if I does,

$$I_{\triangleright} = \frac{1}{2} (I + I_{\text{GJ}}). \quad (17)$$

We allow for the possibility that a gap may form beyond some outer radius R_* . This radius is determined, in the case of a magnetar, by the condition that resonantly scattered X-ray be able to convert directly to electron-positron pairs, and corresponds to the surface where $B = 4B_{\text{Q}}$ (§5). Beyond this gap, a dense polarizable plasma is present and the solution continues to hold in a time-averaged sense.

2.2. Voltage Solution II with an Inner Gap and Pair Multiplicity $\gg 1$

In a super-QED magnetic field, the conversion of gamma rays to pairs generally occurs over a small distance compared with the width of the open magnetic field lines. We therefore focus on a gap with height smaller than $\sim \theta_{\text{open}} R_{\text{NS}}$. Particles flow relativistically through nearly the entire gap width, and so ρ_{\triangleleft} and ρ_{\triangleright} are taken to be constant. The electrostatic potential satisfies the equation

$$\frac{\partial^2 \Phi}{\partial z^2} = -4\pi(\rho_{\triangleright} + \rho_{\triangleleft} - \rho_{\text{GJ}}). \quad (18)$$

Close to the surface of the neutron star, the corotation charge density has an approximately linear dependence on height,

$$\rho_{\text{GJ}} = \rho_{\text{GJ}}(R_{\text{NS}}) \left(1 + A \frac{z}{R_{\text{NS}}} \right). \quad (19)$$

The dimensionless quantity A can be expressed in terms of the frame-dragging coefficient κ (eq. [4]) and the octopole-quadrupole coefficient $\tilde{\kappa}_3$ (eq. [7]) via

$$A \simeq 3\kappa(R_{\text{NS}}) + \tilde{\kappa}_3. \quad (20)$$

(see Appendix A for further details). The pair creation rate is assumed to be zero at at height $z < h$ above the magnetar surface; and to become large at $z > h$. In other words, the density of pairs that are created outside the gap is assumed to become much larger than the change in ρ_{GJ}/e across the gap, within a small distance $z - h \ll h$ from the upper boundary of the gap.

Integrating eq. (18) with respect to z with the boundary conditions $\Phi = d\Phi/dz = 0$ at $z = 0$ and $d\Phi/dz = 0$ at $z = h$ implies a unique value of the charge density inside the gap,

$$\rho = \rho_{\triangleright} + \rho_{\triangleleft} = \rho_{\text{GJ}} \left(z = \frac{1}{2}h \right). \quad (21)$$

The gap solution is

$$\begin{aligned} \rho_{\triangleright} &= \frac{1}{2} \left[\frac{J}{c} + \rho_{\text{GJ}} \left(\frac{h}{2} \right) \right]; \\ \rho_{\triangleleft} &= \frac{1}{2} \left[-\frac{J}{c} + \rho_{\text{GJ}} \left(\frac{h}{2} \right) \right]; \end{aligned}$$

$$\begin{aligned}
E_z(z) &= -\frac{d\Phi}{dz} = 2\pi A \rho_{\text{GJ}}(R_{\text{NS}}) \frac{h^2}{R_{\text{NS}}} \left[\frac{z}{h} - \left(\frac{z}{h}\right)^2 \right]; \\
\Phi(z) &= \Phi_{\text{gap}} \left[3 \left(\frac{z}{h}\right)^2 - 2 \left(\frac{z}{h}\right)^3 \right]; \\
\Phi_{\text{gap}} &\equiv -\frac{\pi}{3} A \rho_{\text{GJ}}(R_{\text{NS}}) \frac{h^3}{R_{\text{NS}}}.
\end{aligned} \tag{22}$$

These expressions for E_z and Φ are very similar to the diode solutions constructed by Arons & Scharlemann (1979) for a space-charge limited flow in a planar geometry, the main difference being that a returning flow of charges is included.

The establishment of the screened state at $z > h$ typically requires a very modest additional potential drop $\Delta\Phi$ compared with the gap voltage (22). Outgoing charges of the sign opposite to ρ_{GJ} must reverse direction so as to maintain $\rho_{\text{<}} + \rho_{\text{>}} = \rho_{\text{GJ}}(r)$. The outgoing charge density has both positive and negative components, $\rho_{\text{>}} = \rho_{\text{>}}^+ + \rho_{\text{>}}^-$, with $|\rho_{\text{>}}^+|, |\rho_{\text{>}}^-| \gg |\rho_{\text{<}}|$. The density of ingoing charges is just sufficient to compensate the difference between J and $\rho_{\text{GJ}}c$,

$$\rho_{\text{<}}(z) = -\frac{1}{2} \left[\frac{J}{c} - \rho_{\text{GJ}}(z) \right]. \tag{23}$$

When the pair creation rate is high at $z > h$, there is a small step in the ingoing charge density at $z = h$,

$$\rho_{\text{<}}(h+\epsilon) - \rho_{\text{<}}(h-\epsilon) = \frac{1}{2} \left[\rho_{\text{GJ}}(h) - \rho_{\text{GJ}}\left(\frac{h}{2}\right) \right] \simeq \frac{A}{4} \left(\frac{h}{R_{\text{NS}}} \right) \rho_{\text{GJ}}(R_{\text{NS}}). \tag{24}$$

We work out a specific example of such a gap in §3, where pair creation is dominated by the resonant scattering of thermal X-rays. When the surface magnetic field is $\sim 10^{14}$ G, particles crossing the gap acquire an energy $e|\Phi_{\text{gap}}| \sim 10^3 - 10^4 m_e c^2$ (depending on the surface temperature).

2.2.1. Sustaining the Low-Voltage Circuit Solution Outside the Gap

The gap solution (22) depends on the ability of the circuit to maintain a configuration with a relatively high particle density outside the gap,

$$n_{\text{>}} + n_{\text{<}} \gg n_{\text{GJ}} \equiv \frac{|\rho_{\text{GJ}}|}{e}, \tag{25}$$

and an approximately charge-balanced state with a low voltage,

$$\rho_{\text{>}}(r) + \rho_{\text{<}}(r) \simeq \rho_{\text{GJ}}(r). \tag{26}$$

In the inner part of the circuit, this second condition can be satisfied if some fraction of the ‘negative’ charges (with a sign opposite to ρ_{GJ}) reverse direction. This is possible because the outgoing primary charges that flow through the gap will create a dense cloud of secondary pairs as they lose energy to resonant drag. The energy spectrum of these secondary particles extends far below the gap voltage. As a result, only a small additional voltage is needed to create the required number of ingoing charges. Indeed, the photons that are resonantly scattered by the outgoing primary charges will continue to create pairs to a much larger distance from the star, where $B \sim 4 \times 10^{12}$ G and the energy of the secondary pairs is $\sim 10 - 100$ times smaller than $e\Phi_{\text{gap}}$ (§4.1).

Screening of the electric field near the outer gap boundary is straightforward in the solution (22), because $E_{\parallel} \rightarrow 0$ inside the upper boundary of the gap even in the absence of pair creation. The minimal pair density that is needed for screening is higher when E_{\parallel} at the first point of pair creation remains comparable to the peak value in the circuit (e.g. Shibata, Miyazaki, & Takahara 1998, 2002). This is the case in the vacuum gap model of Ruderman & Sutherland (1975).

At greater distances from the star, where the cyclotron energy of an electron is $\sim k_B T_{\text{bb}}$, mildly relativistic electrons and positrons feel a very strong drag force (e.g. Thompson & Beloborodov 2005). In this zone, an outgoing charge can reverse direction only in the presence of a relatively strong E_{\parallel} . For the moment, we will neglect the effects of radiation transfer and assume that a large fraction of the outflowing X-rays are unscattered. Near the magnetic pole, an electrostatic potential

$$e d\Phi = -e E_{\parallel} dr = 8.0 \times 10^2 B_{\text{NS},15}^{-1/3} R_{\text{NS},6}^{-1} \left[\frac{(dL_X/d\omega_X) d\omega_X}{10^{35} \text{ ergs s}^{-1}} \right] \left(\frac{\hbar\omega_X}{\text{keV}} \right)^{-2/3} \text{ MeV} \tag{27}$$

just cancels the outward force of resonant scattering on the electrons. The dependence of Φ on radius is plotted in Fig. 1, assuming a blackbody X-ray spectrum. When the magnitude of this potential is much larger than the kinetic energy of the secondary pairs, it is not possible for the circuit to maintain a steady state in which only a fraction of the secondary pairs reverse direction.

A second steady-state circuit solution can, however, be constructed at a somewhat smaller voltage. Here we drop the assumption that all the charges move close to the speed of light. An electric potential just slightly smaller in magnitude than eq. (27) will allow the negative charges to flow *outward* at a speed somewhat below the speed of light, even while the outgoing positive charges remain highly relativistic. The proportions of the current J_+ , J_- that are carried by the positive and negative charges can be left arbitrary, and related to the respective space charge densities via $J_+ \simeq \rho_+ v_+$, $J_- = \rho_- v_-$. Demanding that $J_+ + J_- = J$ and that condition (26) be satisfied, we find

$$\frac{v_-}{c} = \left(1 + \frac{J - \rho_{\text{GJ}}c}{|J_-|} \right)^{-1} = \frac{|J_-|}{J_+ - \rho_{\text{GJ}}c}. \tag{28}$$

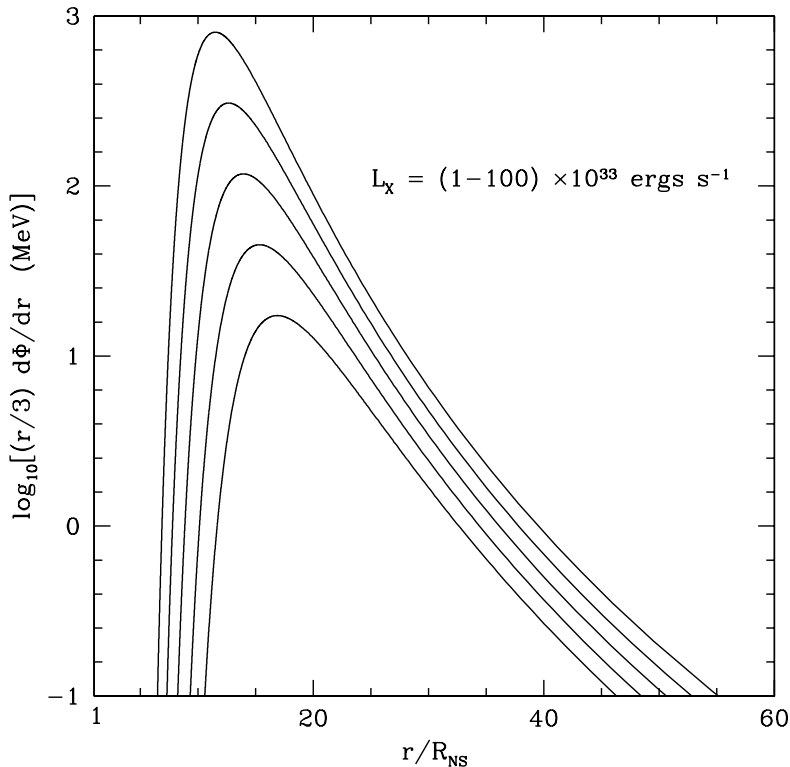


FIG. 1.— Electric potential gradient (given by eq. [27]) that is required to cancel the radiative force exerted by thermal X-rays on a stationary electron or positron. A blackbody spectral distribution is assumed, with emission from the surface of the neutron star ($R_{\text{NS}} = 10$ km) in a single polarization mode. The different curves correspond to X-ray luminosities $(1, 3, 10, 30, 100) \times 10^{33}$ ergs s^{-1} (from bottom to top). If a surface gap emits dense clouds of outgoing pairs, then an electric potential close to this value will develop beyond the radius $\sim (10-15)R_{\text{NS}}$ where the potential drop $e(r/3)d\Phi/dr$ is larger than the minimum energy of the outgoing charges. This relatively weak electric force allows the outflowing plasma to maintain the local charge balance $\rho = \rho_{\text{GJ}}(r)$ in this zone.

This drift speed is indeed smaller than the speed of light, since we are assuming that the total current density $J > \rho_{\text{GJ}}c$ (otherwise, the negative charges are not required to maintain local charge balance within the circuit). The transition between the two circuit solutions occurs at the radius where $eE_{\parallel}r \sim \gamma_{\text{min}}m_e c^2$, where γ_{min} is the minimum Lorentz factor of the secondary pairs.

The fluctuations in the current density are not small when the twist on the open magnetic field lines is dynamic, and there is a significant coupling between the ingoing and reflected torsional waves. The resulting cascade generates very strong current fluctuations, and most of the energy in the fluctuating toroidal magnetic field is deposited in the particles (Thompson & Blaes 1998). In this case, the creation of pairs does not depend on large scale electric fields, and very high pair multiplicities are possible. This type of circuit solution is examined in Thompson (2008).

Finally, we note that our gap solution makes sense only if the outgoing and ingoing charges within the gap have opposite signs. One sees from eq. (22) that this is possible only if J is larger in magnitude than $\rho_{\text{GJ}}(R_{\text{NS}})c$. When J is opposite in sign to $\rho_{\text{GJ}}c$ but smaller in magnitude, then the current can be supplied by an inward subluminal drift of the corotation charge, but only if there is a source of charge in the outer magnetosphere, e.g. associated with an outer gap, or a diversion of current across the magnetospheric boundary.

2.3. Supply of Positive Charges from the Surface of a Magnetar

The current on the open magnetic field lines is supplied mainly by electrons when the spin vector and dipolar magnetic field are aligned ($\mathbf{\Omega} \cdot \mathbf{B} > 0$ and $\rho_{\text{GJ}} < 0$); and by positive charges (ions or positrons) in the case of anti-alignment ($\mathbf{\Omega} \cdot \mathbf{B} < 0$ and $\rho_{\text{GJ}} > 0$). It has been suggested that the observational manifestations of magnetars could be substantially different in the two spin orientations, because heavy ions would be tightly bound to the surface of the star in long molecular chains (Zhang & Harding 2000). Although the binding energy of atoms heavier than oxygen is indeed too high to allow thermionic emission (Thompson et al. 2000), two mechanisms of creating unbound ions are available.

First, downward-moving relativistic electrons trigger a cascade of pairs and gamma rays below the condensed surface. Gamma rays with energies of ~ 20 -30 MeV are created in such a cascade, and are able to knock out protons and neutrons from heavier nuclei. On average $\sim 0.1(\gamma/10^3)$ proton is created per seed relativistic electron of Lorentz factor γ (Beloborodov & Thompson 2007). The pairs created in a surface gap (where $B < 4B_0$) have typical Lorentz factors $\gamma \sim 10^4$ (§3), and the magnitude of the returning charge density can approach ρ_{GJ} if there is a significant mis-match between J and $\rho_{\text{GJ}}c$. In this case, knockout appears marginally effective at supplying a Goldreich-Julian flux of particles. However, the energy of the returning charges is regulated

to $\gamma \sim 10^3$ if $B_{\text{NS}} > 4B_Q$ (§5). A gap may therefore form above the condensed surface with a voltage regulated to the value that gives about ~ 1 proton knocked out per returning charge. This voltage ($\sim 10^{10}$ V) remains too small for the accelerated particles to emit curvature photons in the gamma ray band. An additional population of energetic charges could possibly be created in the outer magnetosphere, with Lorentz factors high enough that returning to the star they suffer negligible resonant drag. (The net kinetic luminosity of these returning charges need only reach $\sim 10^4 m_e c^2 I_{\text{GJ}}/e$, typically $\sim 10^{-3}$ of the spindown luminosity of a magnetar.)

Second, ions can be photodissociated from the molecular chains in the presence of a strong flux of 10-100 keV photons. Most active magnetars are observed to emit such hard X-rays at a rate $\dot{N}_X \sim 10^{42} - 10^{43} \text{ s}^{-1}$ (Kuiper et al. 2004; Mereghetti et al. 2005). The observed spindown of the neutron star implies a much smaller particle flux along its open field lines: a spindown luminosity L_{sd} corresponds to a total Goldreich-Julian flux $\dot{N}_{\text{GJ}} \sim 1 \times 10^{31} L_{\text{sd},33}^{1/2} \text{ s}^{-1}$. This flux arises from a fraction $\pi R_{\text{NS}}/cP = 2 \times 10^{-5} (P/6 \text{ s})^{-1}$ of the neutron star surface. If even one part in a million of the hard X-ray flux is reflected toward a part of the stellar surface that contains the polar cap region, then the photodissociation rate in the polar cap could be high enough to sustain $\dot{N}_{\text{ion}} \sim \dot{N}_{\text{GJ}}$. To put this number in perspective, it will be recalled that a twist angle of $\sim \Delta\phi$ radians in the closed field line region of a magnetar supplies an optical depth $\sim \Delta\phi$ at the electron cyclotron resonance.

Ions themselves are not efficient radiators, so the question then arises as to how pair creation can be spawned in the open field-line region when $\rho_{\text{GJ}} > 0$. The same issue is encountered in electrodynamic models of radio pulsars (e.g. Cheng & Ruderman 1977). The simplest answer is that a state in which the ‘excess’ corotation charge density $\rho_{\text{GJ}} - \rho_{\text{GJ}}^0$ (eq. [5]) is supplied by pair creation is self-sustaining, just as it is in the twisted magnetosphere of a magnetar (Beloborodov & Thompson 2007). The details of how this happens are the subject of §§3 and 5.

3. GAP IN A MAGNETIC FIELD $B < 4B_Q$

The strength of the surface magnetic field has an important influence on the mechanism of pair creation (Beloborodov & Thompson 2007; Thompson 2008). Magnetars are bright thermal X-ray sources, so that relativistic charges produce pairs in copious amounts by the resonant scattering of the X-rays. When $B > 4B_Q$, some resonantly scattered photons are created above the threshold for pair creation, and there is essentially no delay between the positions of scattering and pair conversion. This leads to effective screening of the component of electric field parallel to \mathbf{B} .

The critical field strength for direct pair creation of this type is obtained easily by considering the Landau de-excitation of an electron (or positron) and the energy of the resultant gamma ray. In a frame in which the excited particle is at rest, the gamma ray energy is maximized when it is emitted orthogonal to \mathbf{B} . In this case, the electron receives no recoil, and energy conservation gives $(1 + 2B/B_Q)^{1/2} m_e c^2 = E_\gamma + m_e c^2$. Requiring $E_\gamma > 2m_e c^2$ corresponds to $B > 4B_Q$.

In weaker magnetic fields, direct pair creation by non-resonant scattering is possible at a much reduced cross section. The target photon must have an energy larger than the resonant energy $\hbar\omega'_{\text{res}} = (B/B_Q)m_e c^2$ in the rest frame of the scattering charge. We consider the effects of this process in §3.3.1. Collisions between gamma rays and thermal X-rays can also be important, and are examined in §3.3.2. The resulting zonal structure is summarized in Fig. 2. Many more details and references about pair creation in ultrastrong magnetic fields are given in Thompson (2008).

In this section we consider the case where $B < 4B_Q$ at the surface of the star, so that the conversion of *resonantly* scattered gamma rays to pairs occurs only adiabatically. First, the gamma ray propagates in the curving magnetic field and converts to bound positronium; and, second, the positronium atom is dissociated when one of the constituent charges resonantly scatters an X-ray or absorbs an infrared photon.

3.1. Resonant Scattering of Thermal X-rays

The mean free path for the creation of gamma-rays, and then for the dissociation of the positronium atom, is obtained from the rate of resonant scattering. An X-ray of frequency

$$\omega'_X = \gamma(1 - \beta\mu)\omega_X = \frac{eB}{m_e c} \quad (29)$$

in the rest frame of an electron or positron is scattered with an enhanced cross section. Here μ is the direction cosine of the target photon with respect to the magnetic field (defined so that $\mu > 0$ and $\beta > 0$ when the photon and charge move away from the star). The target photon is strongly aberrated into a direction nearly parallel to \mathbf{B} when the charge moves relativistically ($\beta = v/c \simeq 1$), so that

$$\sigma^{\text{res}}(\omega'_X) \simeq \frac{2\pi^2}{m_e c} \delta\left(\omega'_X - \frac{eB}{m_e c}\right) \quad (30)$$

(Daugherty & Ventura 1978). We focus on the case where the target photons are emitted spherically from the surface of the star, with a temperature T_{bb} and a single polarization state (e.g. Silantve & Iakovlev 1980). The effects of light bending are neglected, so that μ uniformly fills the interval $1 > \mu > \mu_{\text{min}}$, where

$$\mu_{\text{min}} = (1 - R_{\text{NS}}^2/r^2)^{1/2}. \quad (31)$$

One has $\mu_{\text{min}} = 0$ at the surface of the star, and $\mu_{\text{min}} \simeq R_{\text{NS}}^2/2r^2$ at $r \gg R_{\text{NS}}$.

A charge moving radially outward with a Lorentz factor $\gamma_{\triangleright} \gg 1$ scatters X-rays at the rate (Sturmer 1995)

$$\Gamma_{\triangleright}^{\text{res}} = \frac{\alpha_f \Theta_{\text{bb}}^3}{2(B/B_Q)} (1 - \mu_{\text{min}})^2 \tilde{\omega}_{\triangleright}^2 \left| \ln(1 - e^{-\tilde{\omega}_{\triangleright}}) \right| \frac{c}{\lambda_e}. \quad (32)$$

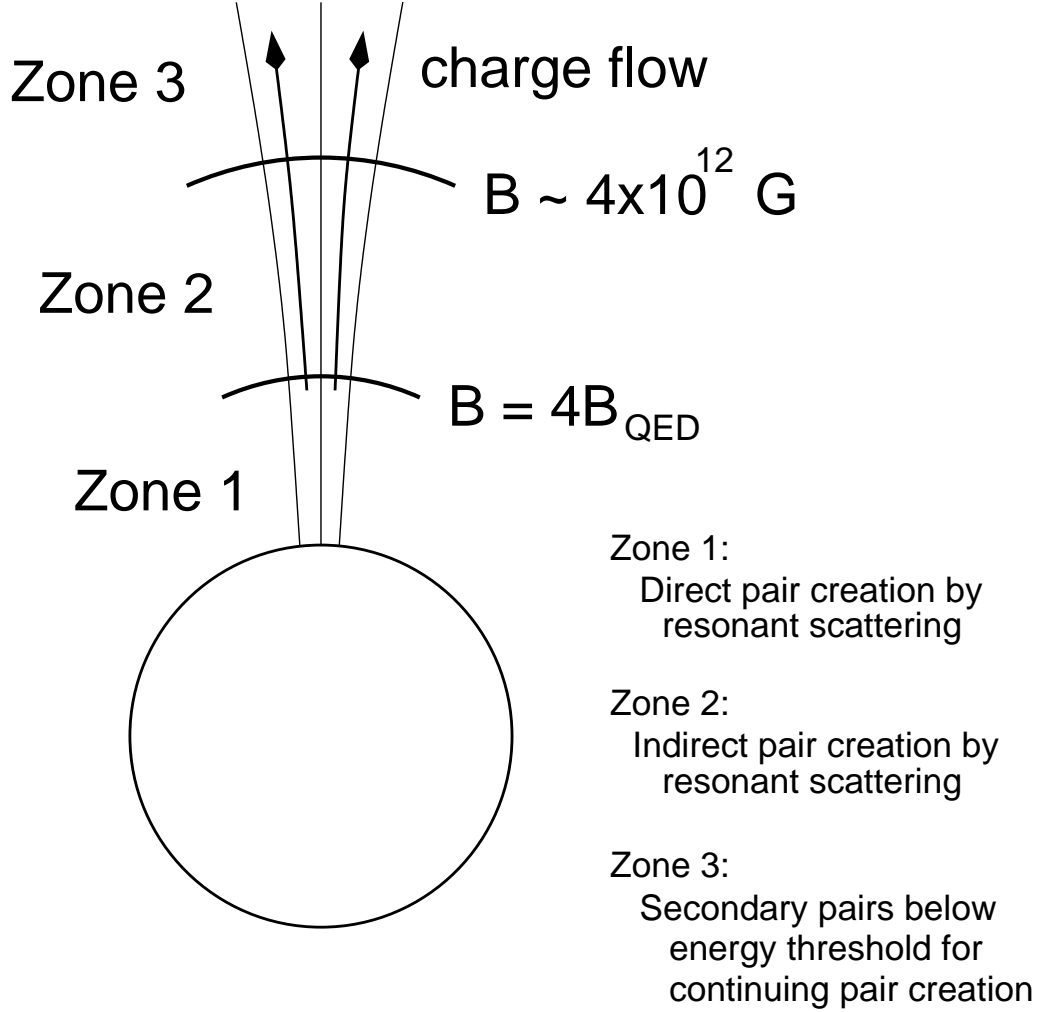


FIG. 2.— Zones of pair creation on the magnetic field lines extending to a large distance from the magnetar surface. The direct conversion of resonantly scattered photons to pairs is restricted to the innermost Zone I, where $B > 4B_{\text{Q}}$. Where the magnetic field is weaker, resonantly scattered photons convert to pairs only after propagating a macroscopic distance. When a dense cloud of pairs forms in a gap close to the surface, large scale electric fields are screened, but new pairs can continue to form as the outflowing particles lose energy to resonant drag, out to the radius where $B \simeq 4 \times 10^{12} \text{ G}$. Secondary modes of pair creation are important inside the gap when the surface temperature $k_{\text{B}} T_{\text{bb}} \gtrsim 0.2 \text{ keV}$. Target photons that are non-resonantly scattered with a reduced cross section can convert directly to pairs in Zone 2, and collisions between resonantly scattered photons and X-rays are important at somewhat higher surface temperatures. See the text for further details.

Here

$$\tilde{\omega}_{\triangleright} \equiv \frac{\hbar\omega_X}{k_{\text{B}}T_{\text{bb}}} = \frac{B/B_{\text{Q}}}{\gamma_{\triangleright}\Theta_{\text{bb}}(1-\mu_{\text{min}})}, \quad (33)$$

is the dimensionless frequency of the target photon at $\mu = \mu_{\text{min}}$. We sometimes use the more compact notation

$$\tilde{\omega}_{\triangleright} \equiv \frac{\gamma_{\triangleright}^{\Theta}}{(1-\mu_{\text{min}})\gamma_{\triangleright}} = 2.3 \times 10^4 (1-\mu_{\text{min}})^{-1} B_{15} \left(\frac{k_{\text{B}}T_{\text{bb}}}{0.5 \text{ keV}} \right)^{-1}. \quad (34)$$

Let us evaluate expression (32) at the surface of the star. An outgoing charge experiences a large number of scatterings if the target photons are drawn from the black body peak ($\tilde{\omega}_{\triangleright} \sim 3$),

$$\frac{R_{\text{NS}}}{c} \Gamma_{\triangleright}^{\text{res}}(R_{\text{NS}}) = 3.9 \times 10^3 B_{\text{NS},15}^{-1} \left(\frac{k_{\text{B}}T_{\text{bb}}}{0.5 \text{ keV}} \right)^3 \tilde{\omega}_{\triangleright}^2 \left| \ln(1 - e^{-\tilde{\omega}_{\triangleright}}) \right|. \quad (35)$$

An analogous expression is obtained for the scattering rate of an ingoing charge,

$$\Gamma_{\triangleleft}^{\text{res}} = \frac{\alpha_f \Theta_{\text{bb}}}{2\gamma_{\triangleleft}^2} \left(\frac{B}{B_Q} \right) \ln \left[\frac{1 - \exp\left(-\frac{B/B_Q}{\gamma_{\triangleleft}(1+\mu_{\text{min}})\Theta_{\text{bb}}}\right)}{1 - \exp\left(-\frac{B/B_Q}{2\gamma_{\triangleleft}\Theta_{\text{bb}}}\right)} \right] \frac{c}{\lambda_e}, \quad (36)$$

which reduces to

$$\Gamma_{\triangleleft}^{\text{res}} = \frac{\alpha_f \Theta_{\text{bb}}^3}{B/B_Q} (1 - \mu_{\text{min}}) f(\tilde{\omega}_{\triangleleft}) \frac{c}{\lambda_e} \quad (37)$$

far from the stellar surface. Here $f(\tilde{\omega}_{\triangleleft}) = \tilde{\omega}_{\triangleleft}^3 (e^{\tilde{\omega}_{\triangleleft}} - 1)^{-1}$,

$$\tilde{\omega}_{\triangleleft}(\gamma_{\triangleleft}) = \frac{\gamma_{\triangleleft}^{\ominus}}{\gamma_{\triangleleft}}, \quad (38)$$

and

$$\gamma_{\triangleleft}^{\ominus} = \frac{B/B_Q}{2\Theta_{\text{bb}}} = 1.2 \times 10^4 B_{15} \left(\frac{k_B T_{\text{bb}}}{0.5 \text{ keV}} \right)^{-1}. \quad (39)$$

3.2. Basic Gap Solution

We now determine the basic properties of the gap solution outlined in §2.2. In this solution, the total current density is allowed to exceed $\rho_{\text{GJ}}c$, with a returning flux of charges of the sign opposite to ρ_{GJ} supplying a significant fraction of J . The gap voltage is then proportional to the gradient in ρ_{GJ} along the open magnetic field lines,

$$|\Phi_{\text{gap}}| = \frac{\pi}{3} \frac{d\rho_{\text{GJ}}}{dr} h^3 \equiv A \frac{\pi}{3} \frac{\rho_{\text{GJ}} h^3}{R_{\text{NS}}}, \quad (40)$$

just as it is in models of pulsar circuits with a steady, space-charge limited flow (Arons & Scharlemann 1979). In contrast with models of pulsar polar caps with realistic pair creation (e.g. Hibschan & Arons 2001a), the thickness h of the gap can self-consistently be assumed small compared with the width of the open magnetic field lines, $h \ll \theta_{\text{open}} R_{\text{NS}}$.

We start with the simplest solution, in which Φ_{gap} and h are determined by i) the gradient in ρ_{GJ} away from the neutron star surface; and ii) the degree of curvature of the magnetic field lines (Fig. 3). This solution is valid if pair creation occurs mainly by the adiabatic conversion of gamma rays off the magnetic field, and the charges streaming through the gap feel a negligible drag force due to resonant scattering. It turns out that both of these conditions are satisfied if the surface temperature is below a critical value, $k_B T_{\text{bb}} \lesssim 0.15 - 0.2 \text{ keV}$.

The thickness of the gap is determined by summing three quantities, and then minimizing this sum: i) the distance Δz for an outgoing particle to be accelerated to the Lorentz factor γ at which it resonantly scatters a background photons; ii) the distance $\Delta z'$ for the resonantly scattered photon to convert to a pair; and iii) the distance $\Delta z''$ for one of the created particles to reverse direction in the background potential, thereby polarizing the plasma within the gap. This procedure is self-consistent when the mean number of scattered photons per outgoing charge satisfies,

$$\mathcal{M}_{\gamma} \gg \frac{\Delta\rho_{\triangleleft}}{\rho_{\text{GJ}}} = \frac{Ah}{4R_{\text{NS}}}. \quad (41)$$

Here $\Delta\rho_{\triangleleft} = \rho_{\triangleleft}(h+\epsilon) - \rho_{\triangleleft}(h-\epsilon)$ is the shift in the ingoing charge density across the outer boundary of the gap, and is given by eq. (24). The right-hand side of eq. (41) is small, and so this condition is consistent with weak drag. In this case, the gap thickness depends only weakly on the density of target photons, and we can take the energy of the resonantly scattered photon to be the maximum possible energy. In a super-QED magnetic field, this is a sizeable fraction of the kinetic energy of the scattering charge,

$$E_{\gamma}(\text{max}) = \frac{2B/B_Q}{1+2B/B_Q} \gamma m_e c^2. \quad (42)$$

In the regime of weak drag, multiple scatterings are rare and a scattering particle attains its kinetic energy $\gamma m_e c^2$ at a potential drop $\Delta\Phi \simeq \gamma m_e c^2 / e$ from the gap boundary. After conversion of the gamma-ray to a pair, one of the two outgoing charges will reverse direction after the particles pass through an additional potential drop $\Delta\Phi'' \simeq \frac{1}{2} \gamma m_e c^2 / e$. The relation between particle energy and position within the gap is

$$\frac{\gamma}{\gamma_{\text{max}}} = 3 \left(\frac{z}{h} \right)^2 - 2 \left(\frac{z}{h} \right)^3 \equiv \phi \left(\frac{z}{h} \right), \quad (43)$$

where

$$\gamma_{\text{max}} = \frac{A}{6} \left(\frac{\Omega R_{\text{NS}}}{c} \right) \frac{e B_{\text{NS}} R_{\text{NS}}}{m_e c^2} \left(\frac{h}{R_{\text{NS}}} \right)^3 \equiv K_{\text{gap}} \left(\frac{h}{R_{\text{NS}}} \right)^3. \quad (44)$$

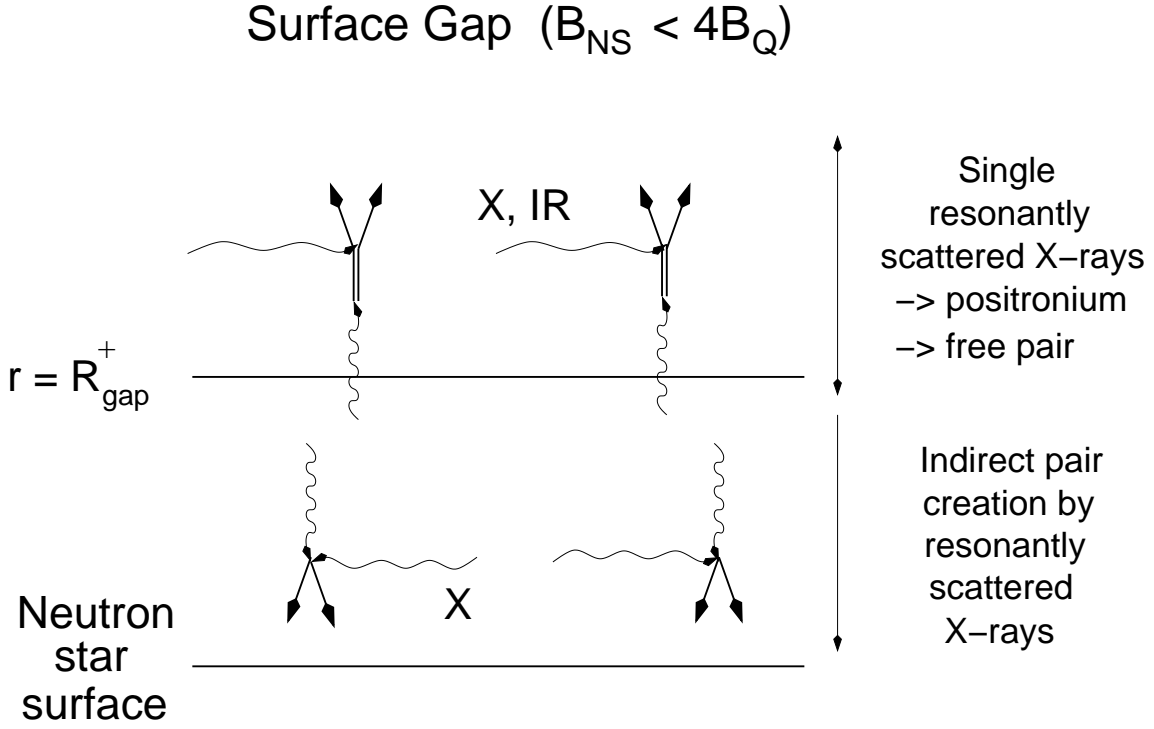


FIG. 3.— Structure of a gap at the surface of a neutron star with a polar magnetic field $B_{\text{NS}} < 4B_{\text{Q}}$. Some key modes of pair creation are labelled. Outgoing particles resonantly upscatter thermal X-rays that are emitted from the surface of the neutron star. When the surface temperature is lower than ~ 0.2 keV, the width of the gap is set by the conversion of these gamma rays to free pairs off the magnetic field. (The gamma ray first converts to bound positronium, which is then rapidly dissociated when one of the charges resonantly scatters an ambient X-ray.) A fraction of the gamma rays within the gap can convert to pairs by colliding with an X-ray before reaching the threshold energy for single-photon pair creation, and direct pair creation by non-resonant scattering is also important. The gap voltage is lowered by these effects when $k_{\text{B}}T_{\text{bb}} \gtrsim 0.2$ keV.

(see eq. [22]). The position of scattering is a distance Δz from one boundary of the gap, and the position of pair conversion is a distance $\Delta z''$ from the other boundary, where

$$\phi\left(\frac{\Delta z}{h}\right) = \frac{\gamma}{\gamma_{\text{max}}}; \quad \phi\left(\frac{\Delta z''}{h}\right) \simeq \frac{\gamma/2}{\gamma_{\text{max}}}. \quad (45)$$

As the thickness of the gap shrinks, so does the voltage and the particle Lorentz factor. The delay between gamma ray emission and pair conversion therefore plays an essential role in stabilizing the gap. The conversion distance $\Delta z'$ for the gamma ray scales inversely with γ , and so increases with decreasing h ,

$$\Delta z' = \frac{2m_e c^2}{E_{\gamma}(\text{max})} R_C = \frac{2}{\gamma} \left(\frac{2B/B_{\text{Q}}}{1+2B/B_{\text{Q}}} \right)^{-1} R_C. \quad (46)$$

Here R_C is the curvature radius of the magnetic field lines, which in the case of strong field curvature is given by eq. (A9). The equilibrium gap width can be obtained by setting

$$\frac{\partial h}{\partial \gamma} = \frac{\partial}{\partial \gamma} (\Delta z + \Delta z' + \Delta z'') = 0. \quad (47)$$

Differentiating eqs. (45) and (46) with respect to γ , and substituting into eq. (47) gives

$$\frac{1}{\phi'(\Delta z/h)} + \frac{1}{2\phi'(\Delta z''/h)} = \frac{\Delta z'/h}{\phi(\Delta z/h)}. \quad (48)$$

Combining this with the relations $\phi(\Delta z/h) = 2\phi(\Delta z''/h)$ and $\Delta z' = h - \Delta z - \Delta z''$, we obtain the solution

$$\Delta z \simeq 0.38h; \quad \Delta z'' \simeq 0.25h, \quad (49)$$

and

$$\gamma_{\text{max}} = 17.5 \left(\frac{2B/B_{\text{Q}}}{1+2B/B_{\text{Q}}} \right)^{-1} \frac{R_C}{h}. \quad (50)$$

Displaced Gap ($B_{NS} > 4B_Q$)

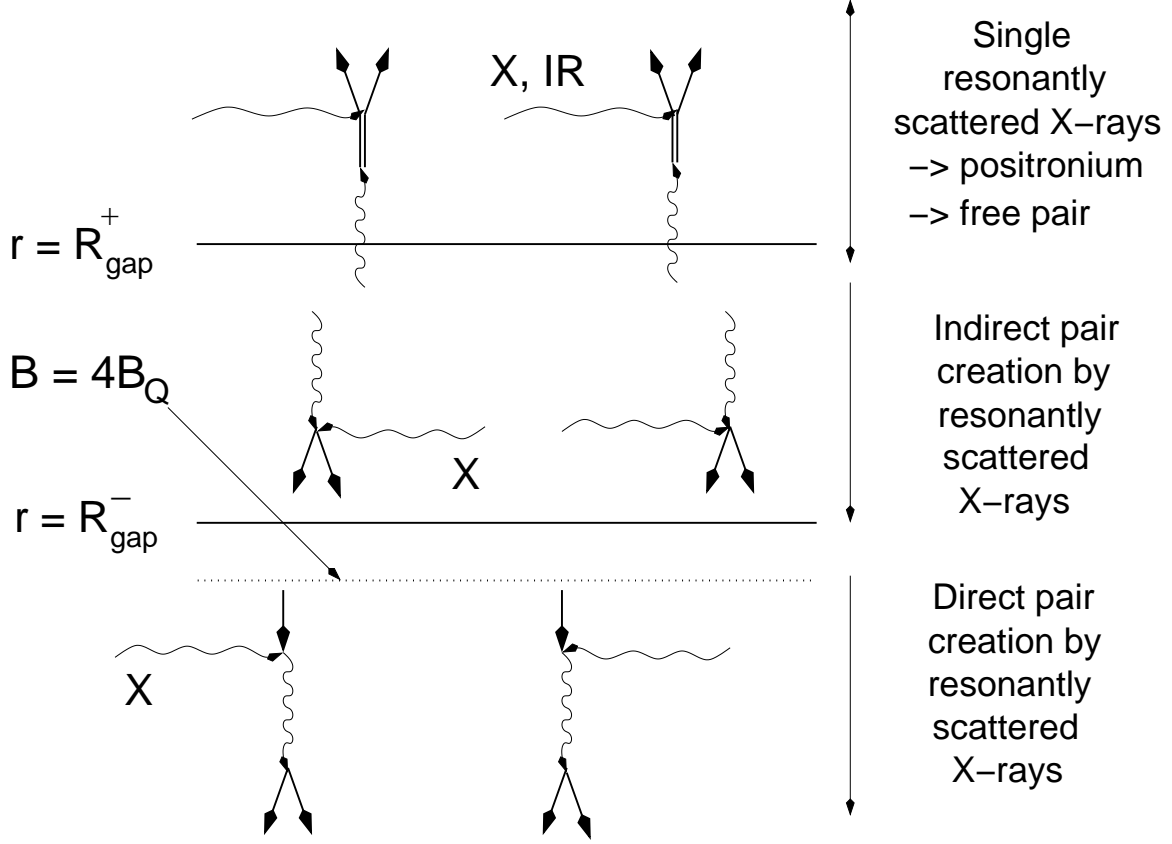


FIG. 4.— Possible structure of a gap whose inner boundary is shifted just outside the surface $B_{NS} = 4B_Q$, in the case of a magnetar with a polar magnetic field $B_{NS} > 4B_Q$. The existence of such a gap depends on the non-linear development of the two-stream instability within the circuit.

Substituting again for γ_{\max} gives the equilibrium gap width,

$$\begin{aligned} \frac{h}{R_{NS}} &= \left[\frac{K_{\text{gap}}}{17.5} \left(\frac{2B/B_Q}{1+2B/B_Q} \right) \right]^{-1/4} \\ &= \frac{2.7 \times 10^3}{\mathcal{F}^{1/4}(B)} \frac{R_{NS,6}^{1/2}}{A^{1/4} B_{NS,14}^{1/4}} \left(\frac{P}{6 \text{ s}} \right)^{1/4} \left(\frac{R_C}{R_{NS}} \right)^{1/4} \quad \text{cm,} \end{aligned} \quad (51)$$

and voltage

$$\gamma_{\max} = \frac{e|\Phi_{\text{gap}}|}{m_e c^2} = \frac{6.5 \times 10^3}{\mathcal{F}^{3/4}(B)} A^{1/4} B_{NS,14}^{1/4} R_{NS,6}^{1/2} \left(\frac{P}{6 \text{ s}} \right)^{-1/4} \left(\frac{R_C}{R_{NS}} \right)^{3/4}, \quad (52)$$

where

$$\mathcal{F}(B) \equiv \frac{2B/B_Q}{1+2B/B_Q}. \quad (53)$$

We now consider the number of photons that are resonantly upscattered by the outgoing charges. The scattering rate is, in fact, somewhat higher for the ingoing charges (which see photons moving toward them nearly head on). The maximum energy of the resonantly scattered photons is, however, the same for particles moving in both directions, and the distribution of kinetic energies within the gap is symmetric between the two directions.⁴ The gap width, as determined by the minimization procedure (47), is therefore independent of the direction in which the scattering charges are moving.

⁴ Each outflowing particle scatters X-rays at a modest rate. We therefore neglect the effect of the recoil on the motion of a typical outgoing particle.

A simple estimate of the energy of the gamma ray is obtained by viewing the scattering process as resonant absorption followed by de-excitation. The absorbing charge decelerates from a Lorentz factor γ to $\gamma_1 < \gamma$, which is found from the equation of energy conservation, $\hbar\omega_X + \gamma m_e c^2 = \gamma_1 E_B$, where $E_B = (1 + 2B/B_Q)^{1/2} m_e c^2$ is the energy of the first Landau level. This gives (neglecting the small energy $\hbar\omega_X$)

$$\gamma_1 = \frac{\gamma m_e c^2}{E_B} = \gamma \left(1 + 2\frac{B}{B_Q}\right)^{-1/2}. \quad (54)$$

The final Lorentz factor of the electron, when it returns to the ground state, equals γ_1 only if the de-excitation photon is emitted perpendicular to \mathbf{B} in the electron frame. Otherwise there is a recoil effect whose sign depends on the photon direction. If we adopt γ_1 as an estimate of the mean final Lorentz factor, the typical loss in scattering is⁵

$$\Delta\gamma \simeq \gamma - \gamma_1 \equiv f_{\text{recoil}}\gamma, \quad (55)$$

where

$$f_{\text{recoil}} = 1 - \left(1 + 2\frac{B}{B_Q}\right)^{-1/2}. \quad (56)$$

The number of scatterings per outgoing particle is distributed over gamma ray energy $E_\gamma = f_{\text{recoil}}\gamma m_e c^2$ according to

$$E_\gamma \frac{d\mathcal{M}_\gamma}{dE_\gamma} \Big|_{\triangleright} = \gamma \frac{d\mathcal{M}_\gamma}{d\gamma} \Big|_{\triangleright} = \frac{\gamma m_e c \Gamma_{\triangleright}^{\text{res}}}{eE_z}, \quad (57)$$

where we take $\mu_{\text{min}} = 0$ at the surface of the star. Substituting eqs. (22), (32), (51), and (52) gives

$$\begin{aligned} E_\gamma \frac{d\mathcal{M}_\gamma}{dE_\gamma} \Big|_{\triangleright} &= 1.46 \frac{\alpha_f \Theta_{\text{bb}}^2}{\gamma_{\text{max}}^2 \mathcal{F}(B)} \left(\frac{R_C}{\lambda_e}\right) \frac{\tilde{\omega}_{\triangleright} |\ln(1 - e^{-\tilde{\omega}_{\triangleright}})|}{(z/h) - (z/h)^2} \\ &= \frac{6.2 \mathcal{F}^{1/2}(B)}{A^{1/2} B_{\text{NS},14}^{1/2}} \left(\frac{k_B T_{\text{bb}}}{0.5 \text{ keV}}\right)^2 \left(\frac{P}{6 \text{ s}}\right)^{1/2} \left(\frac{R_C}{R_{\text{NS}}}\right)^{-1/2} \frac{\tilde{\omega}_{\triangleright} |\ln(1 - e^{-\tilde{\omega}_{\triangleright}})|}{(z/h) - (z/h)^2}, \end{aligned} \quad (58)$$

where the normalized energy of the target photon is

$$\tilde{\omega}_{\triangleright} = \frac{B/B_Q}{\gamma \Theta_{\text{bb}}} = 0.36 \left(\frac{\gamma_{\text{max}}}{\gamma}\right) \frac{\mathcal{F}^{3/4}(B) B_{\text{NS},14}^{3/4}}{A^{1/4} R_{\text{NS},6}^{1/2}} \left(\frac{k_B T_{\text{bb}}}{0.5 \text{ keV}}\right)^{-1} \left(\frac{P}{6 \text{ s}}\right)^{1/4} \left(\frac{R_C}{R_{\text{NS}}}\right)^{-3/4}. \quad (59)$$

The analogous expression for ingoing charges is obtained from eq. (37) for the scattering rate $\Gamma_{\triangleleft}^{\text{res}}$; one finds

$$E_\gamma \frac{d\mathcal{M}_\gamma}{dE_\gamma} \Big|_{\triangleleft} = \left[\frac{\ln(1 - e^{-\tilde{\omega}_{\triangleright}/2})}{\ln(1 - e^{-\tilde{\omega}_{\triangleright}})} - 1 \right] E_\gamma \frac{d\mathcal{M}_\gamma}{dE_\gamma} \Big|_{\triangleright}, \quad (60)$$

where we have made use of the relations $\tilde{\omega}_{\triangleleft} = \frac{1}{2}\tilde{\omega}_{\triangleright}$ for $\mu_{\text{min}} = 0$ (eqs. [33], [38]).

A useful measure of resonant scattering within a gap is the relative magnitude of the electric force and the drag force due to scattering,

$$\frac{F_{\text{drag}}^{\triangleright,\triangleleft}}{eE_{\parallel}} = f_{\text{recoil}} \frac{d\mathcal{M}_\gamma}{d\ln E_\gamma} \Big|_{\triangleright,\triangleleft}. \quad (61)$$

This quantity is plotted in Fig. 5 as a function of blackbody temperature for polar magnetic fields $B_{\text{NS}} = B_Q$ and $3B_Q$. The mean energy of the resonantly scattered photons is reduced by drag when $F_{\text{drag}}/e|E_{\parallel}| \gtrsim 1$ at $z \sim \frac{1}{2}h$. The critical temperature T_{drag} above which this inequality is satisfied is plotted in Fig. 6. Although the drag formally is important when $k_B T_{\text{bb}} \gtrsim 0.2 \text{ keV}$, we find that other pair creation mechanisms will reduce the gap voltage in that temperature range and thereby reduce the effects of drag.

The possibility of a surface gap in a magnetic field stronger than $4B_Q$ deserve some comment. In this case most resonantly scattered X-rays will quickly convert to pairs, so that $\Delta' \simeq 0$. The gap structure examined here then appears to be unstable to collapse to small h , and it may disappear entirely. On the other hand, a self-consistent gap structure may be sustained outside the surface where $B = 4B_Q$, with properties very similar to those described here (Fig. 4).

3.3. Reduction of the Gap Voltage by Secondary Modes of Pair Creation

The gap voltage can be reduced by additional modes of pair creation, which we now consider. Gamma rays created by the resonant scattering of thermal X-rays can collide with the X-rays to form free pairs, before they reach the threshold for single-photon pair creation (see Zhang & Qiao 1998 for a discussion of this process in the context of ordinary radio pulsars). Higher

⁵ It equals $\frac{2}{3}\gamma$ for $B = 4B_Q$ and $\simeq 0.85\gamma$ for $B = 10^{15} \text{ G}$. The lost energy is carried by the scattered photon. It is shared between two new particles when the photon converts to a pair. Each particle in the created pair therefore has a typical kinetic energy $\sim 0.3\text{--}0.4\gamma m_e c^2$ in the direction of the scattering charge.

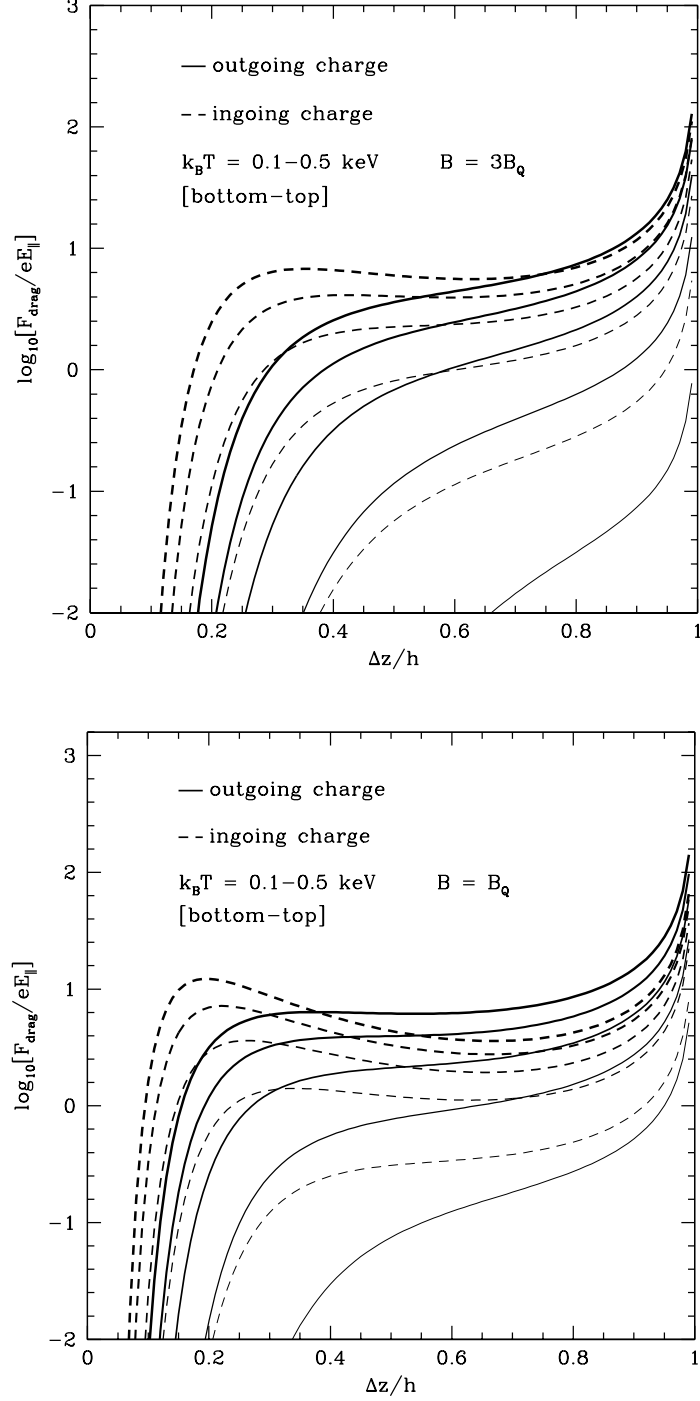


FIG. 5.— Ratio of drag force due to resonant scattering, and the accelerating electric force, within the gap solution given by eq. (22). The forces on the outgoing and ingoing charges are evaluated separately, as a function of the distance from the injection radius ($z = 0, h$ respectively). The results are displayed for surface magnetic fields $B_{\text{NS}} = B_Q$ and $3B_Q$. Each set of five curves corresponds to blackbody temperatures $k_B T_{\text{bb}} = 0.1, 0.2, 0.3, 0.4,$ and 0.5 keV (thicker curves representing higher temperatures). We choose parameters $A = 1, R_{\text{NS}} = 10 \text{ km}, R_C = R_{\text{NS}}$ and $P = 6 \text{ s}$.

energy gamma rays will also be emitted even when $B < 4B_Q$, with a cross section comparable to the Klein-Nishina value. The emission rate is lower than for resonant scattering, but the conversion to a pair is almost immediate. This second process turns out to impose the stronger limitations on the thermal X-ray flux at low temperatures, and we discuss it first.

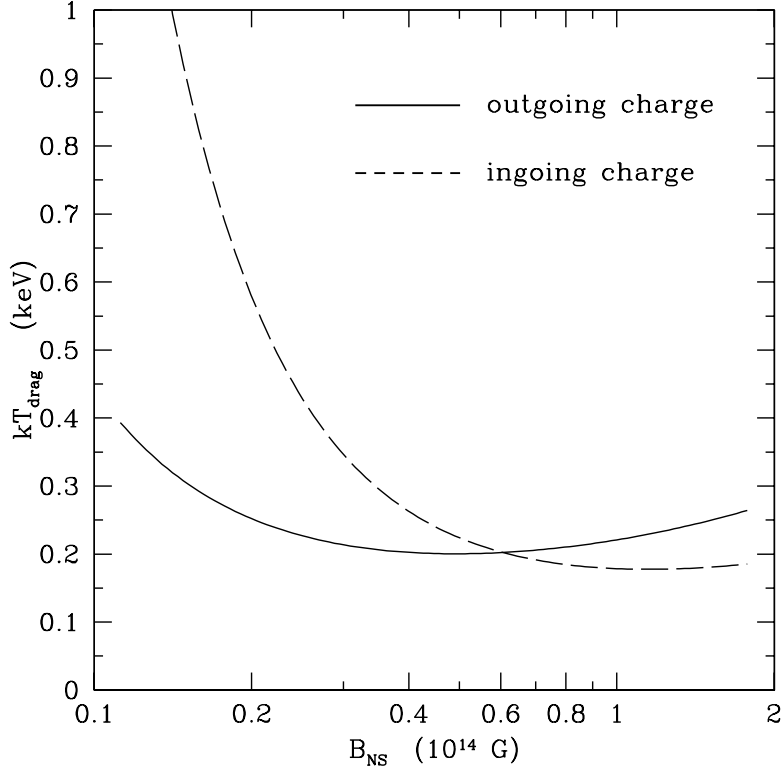


FIG. 6.— Critical blackbody X-ray temperature above which charges flowing through the middle of the gap (22) feel a drag force equal to eE_{\parallel} , as a function of magnetic field in the gap. We choose parameters $A = 1$, $R_{\text{NS}} = 10$ km, $R_C = R_{\text{NS}}$ and $P = 6$ s.

The rate of pair creation integrated through the gap must not exceed a critical value,

$$\frac{e}{c} \int_0^h dz \dot{n}_{\pm} < \frac{h}{4} \frac{d\rho_{\text{GJ}}}{dr} \equiv \frac{A}{4} \left(\frac{h}{R_{\text{NS}}} \right) \rho_{\text{GJ}}, \quad (62)$$

which corresponds to a net production of negative charges equal to the jump (24) in the ingoing charge density at the outer boundary of the gap. We focus here on a gap situated at the surface of the neutron star, where outgoing and ingoing charges make significant contributions to the integral (62).

3.3.1. Direct Pair Creation through Non-resonant Scattering

We now work out the kinematic constraints on direct pair creation by non-resonant scattering. The cross section for scattering of a gamma ray by an electron is well approximated by the Klein-Nishina expression when $\omega \gtrsim 3eB/m_e c$ (Gonthier et al. 2000). The rate of Klein-Nishina scattering of peak photons is given by (Blumenthal & Gould 1970)

$$\Gamma_{\triangleright}^{\text{KN}} = (1.65) \frac{\alpha_f^2 \Theta_{\text{bb}}^2}{4\pi\gamma} \ln(\gamma\Theta_{\text{bb}}) \frac{c}{\lambda_e} \quad (63)$$

(assuming that the thermal photons are emitted in a single polarization mode). Relative to the rate of resonant scattering of low-energy photons from the Rayleigh-Jeans tail, this is

$$\frac{\Gamma_{\triangleright}^{\text{KN}}}{\Gamma_{\triangleright}^{\text{res}}} \sim 2 \times 10^{-3} \left(\frac{\gamma}{\gamma_{\triangleright}^{\ominus}} \right) \frac{\ln[(\gamma/\gamma_{\triangleright}^{\ominus})(B/B_Q)]}{\ln(\gamma/\gamma_{\triangleright}^{\ominus})} \quad (\gamma > \gamma_{\triangleright}^{\ominus}). \quad (64)$$

This expression holds in sub-QED magnetic fields for $\gamma > \gamma_{\triangleright}^{\ominus}(B/B_Q)^{-1}$.

In the rest frame of the electron, the X-ray photon has an initial energy $\hbar\omega'_X \simeq \gamma(1 - \cos\theta_{kB})\hbar\omega_X$ and is taken to scatter through an angle $\theta'_{kB,2}$ with respect to \mathbf{B} . The threshold condition for direct pair creation following the scattering is

$$\hbar\omega'_{X,2} \sin\theta'_{kB,2} > 2m_e c^2, \quad (65)$$

where

$$\omega'_{X,2} = \frac{\omega'_X}{1 + (\hbar\omega'_X/m_e c^2)(1 - \cos\theta'_{kB,2})} \quad (66)$$

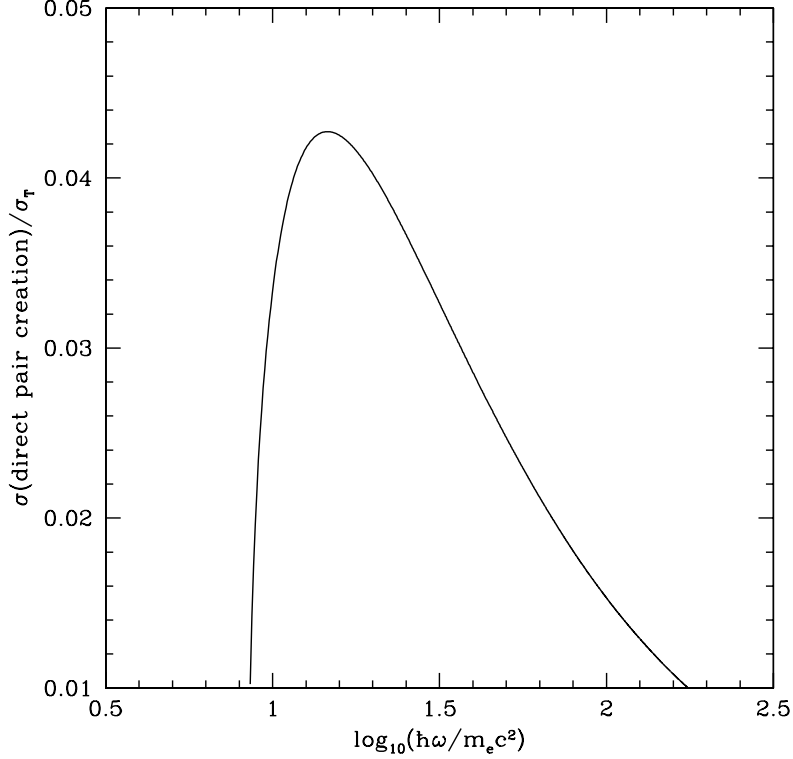


FIG. 7.— Klein-Nishina cross section integrated over scattering angles that result in an outgoing photon above the threshold for direct pair creation, $\sin\theta'_{kB,2}\hbar\omega'_{X,2} > 2m_e c^2$. The incident photon is assumed to propagate parallel to the magnetic field, which has only a modest effect on the cross section when the photon energy is larger than $\sim 3\hbar eB/m_e c$. Polarization effects are important only when the magnetic field is close to the threshold value $4B_Q$ for direct pair creation following Landau de-excitation. In that case, an E-mode photon has a significantly higher threshold energy for pair creation than does an O-mode photon. The threshold condition for pair creation is essentially polarization independent when $B \ll 4B_Q$.

is the frequency of the photon after scattering. The quantity on the left-hand side of eq. (65) is maximized when

$$\cos\theta'_{kB,2} = \frac{1}{1 + m_e c^2 / \hbar\omega'_X}. \quad (67)$$

The minimum energy of the incident photon for direct pair creation is

$$\hbar\omega'_X = (4 + \sqrt{20})m_e c^2. \quad (68)$$

Approximating $1 - \cos\theta_{kB} \simeq \frac{1}{2}(r/R_{NS})^{-2}$ in the frame of the star gives the threshold energy

$$\gamma = \frac{4(2 + \sqrt{5})m_e c^2}{\hbar\omega_X} \left(\frac{r}{R_{NS}} \right)^2 \quad (69)$$

for direct pair creation by a relativistic electron moving away from the star.

More energetic photons will scatter into a state that can convert directly to an electron positron pair over some range of scattering angles,

$$\frac{4x}{5} - \frac{2}{5}\sqrt{\frac{5}{4} - x^2} < \cos\theta'_{kB,2} < \frac{4x}{5} + \frac{2}{5}\sqrt{\frac{5}{4} - x^2}, \quad (70)$$

where $x \equiv 1 + m_e c^2 / \hbar\omega'_X$. The Klein-Nishina cross section integrated over this range of angles is plotted as a function of incident photon energy in Fig. 7. One sees that this integrated cross section peaks over the range of frequencies $\hbar\omega'_X = (10-20)m_e c^2$. Denoting it by $\sigma_{n\text{-res}}$, we make the approximation that the scattering is concentrated at a given frequency $\hbar\omega_0 \simeq 16m_e c^2$, so that $\sigma_{n\text{-res}}(\omega'_X) = \sigma_{n\text{-res}}^0 \omega'_X \delta(\omega'_X - \omega_0)$. Here $\sigma_{n\text{-res}}^0 = 0.04\sigma_T$. (It will turn out that the rate of direct pair creation off a thermal photon field, maximized with respect to γ , is independent of ω_0 .)

The rate of direct pair creation can then be written as

$$\Gamma_{n\text{-res}}^{\gt,\lt} = \int d\omega_X \int_{\mu_{\min}}^1 2\pi d\mu \frac{I_{\omega_X}}{\hbar\omega_X} (1 \mp \mu) \sigma_{n\text{-res}}(\omega_X, \mu, \gamma). \quad (71)$$

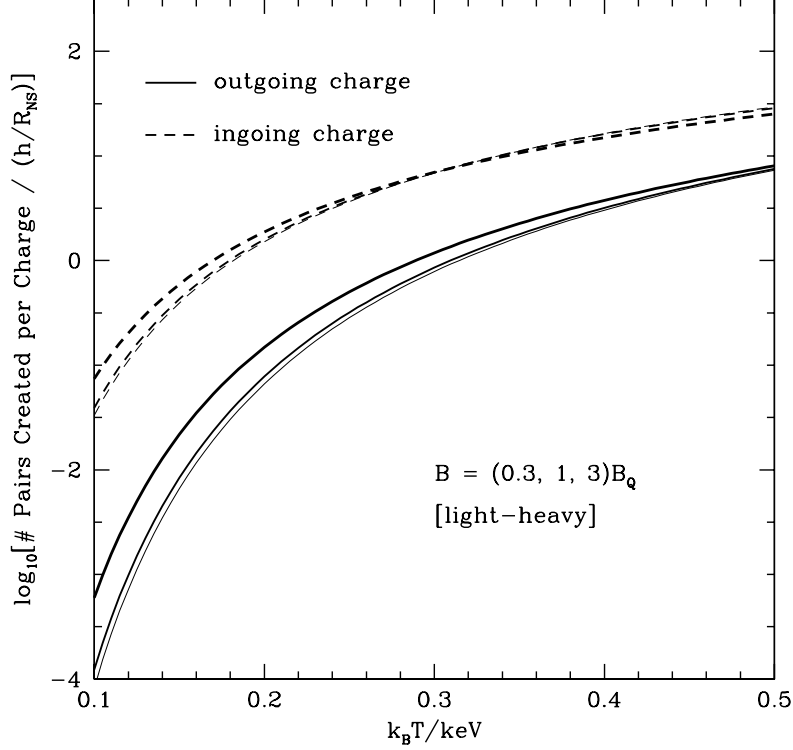


FIG. 8.— Number of pairs that are created by the direct conversion of non-resonantly scattered photons, within the gap given by eq. (22). The background magnetic field is weaker than the critical value $4B_Q$ for direct pair creation by resonantly scattered photons. The contributions from outgoing and ingoing charges are evaluated separately. The gap voltage is reduced by this process when eq. (87) is satisfied. Each set of three curves corresponds to magnetic fields $0.3B_Q$, B_Q and $3B_Q$ (thicker curves representing stronger fields). We choose parameters $\sigma_{n\text{-res}}^0 = 0.04 \sigma_T$, $\hbar\omega_0 = 16 m_e c^2$, $A = 1$, $R_{\text{NS}} = 10$ km, $R_C = R_{\text{NS}}$ and $P = 6$ s.

Here ω_X and I_{ω_X} are the frequency and intensity of the thermal X-rays, which we assume to be emitted from the neutron star surface in a single polarization mode (the extraordinary mode),

$$I_{\omega_X} = \frac{\hbar\omega_X^3}{(2\pi)^3 c^2} \left[\exp\left(\frac{\hbar\omega_X}{k_B T_{\text{bb}}}\right) - 1 \right]^{-1}. \quad (72)$$

We evaluate this expression for values of γ where $\omega = \omega_0/\gamma(1 \mp \mu)$ sits in the Wien tail of the thermal X-ray distribution.

$$\Gamma_{n\text{-res}}^{\triangleright}(r, \gamma) = \frac{k_B T_{\text{bb}}}{\hbar} \left(\frac{\omega_0^2 \sigma_{n\text{-res}}^0}{4\pi^2 c^2 \gamma^2} \right) \exp\left[-\frac{\hbar\omega_0/k_B T_{\text{bb}}}{\gamma(1 - \mu_{\text{min}})} \right] \quad (73)$$

for an outgoing charge, and

$$\Gamma_{n\text{-res}}^{\triangleleft}(r, \gamma) = \frac{k_B T_{\text{bb}}}{\hbar} \left(\frac{\omega_0^2 \sigma_{n\text{-res}}^0}{4\pi^2 c^2 \gamma^2} \right) \left\{ \exp\left[-\frac{\hbar\omega_0/k_B T_{\text{bb}}}{2\gamma} \right] - \exp\left[-\frac{\hbar\omega_0/k_B T_{\text{bb}}}{\gamma(1 + \mu_{\text{min}})} \right] \right\} \quad (74)$$

for an ingoing charge.

The number of pairs that are created within the gap by each charge is obtained by evaluating the expression

$$N_{\pm} \Big|_{\triangleright, \triangleleft} = \int_0^h \frac{dz}{c} \Gamma_{n\text{-res}}^{\triangleright, \triangleleft}, \quad (75)$$

where the Lorentz factor at height z is given by eq. (43). The results are displayed in Fig. 8, where we have removed a factor h/R_{NS} .

3.3.2. Collisions between X-rays and Gamma-rays

The rate of pair creation by photon collisions can be written in terms of an integral over the distributions of the gamma rays and the secondary target X-rays,

$$n_{\pm} \Big|_{\triangleright} = \int d\omega_{\gamma} \int d\omega_X \int 2\pi d\mu_X \left(\frac{d\mathcal{M}_{\gamma}}{d\omega_{\gamma}} \Big|_{\triangleright} f_{\triangleright} n_{\text{GJ}} \right) \left(\frac{I_{\omega_X}}{\hbar\omega_X} \right) \sigma_{X\gamma}(\omega_{\gamma}, \omega_X, \mu_X) (1 - \mu_X). \quad (76)$$

Here $\omega_\gamma = E_\gamma/\hbar$ and ω_X are the frequency of the gamma ray and the target X-rays. This expression applies to the case where the gamma rays are emitted parallel to \mathbf{B} by outgoing relativistic charges. A similar expression applies to the case where the gamma rays are emitted by ingoing relativistic charges: one replaces f_{\triangleright} with f_{\triangleleft} and $1 - \mu_X$ with $1 + \mu_X$. Here

$$f_{\triangleright} = \frac{n_{\triangleright}}{n_{\text{GJ}}} = \frac{1}{2} \left(1 + \frac{J}{\rho_{\text{GJ}} c} \right); \quad f_{\triangleleft} = \frac{n_{\triangleleft}}{n_{\text{GJ}}} = \frac{1}{2} \left(\frac{J}{\rho_{\text{GJ}} c} - 1 \right). \quad (77)$$

The multiplicity $d\mathcal{M}_\gamma/dE_\gamma$ of resonantly scattered gamma rays is given respectively by eqs. (58) and (60) in these two cases.

We make the approximation that the cross section for collisions between X-rays and curvature gamma rays is concentrated at the threshold $\omega\omega_X(1 - \mu_X) = 2m_e^2$, namely

$$\sigma_{X\gamma}(\omega_\gamma, \omega_X, \mu_X) = \sigma_{X\gamma}^0 \omega_\gamma \omega_X (1 - \mu_X) \delta \left[\omega_\gamma \omega_X (1 - \mu_X) - 2 \left(\frac{m_e c^2}{\hbar} \right)^2 \right]. \quad (78)$$

The value of $\sigma_{X\gamma}^0$ depends on the shape of the two photon spectra: following eq. (41) of Thompson (2008), we normalize to $\sigma_{X\gamma} = 0.02 \sigma_T$ (corresponding to a magnetic field $B = 4B_Q$). The integrals over ω_X, μ_X in eq. (76) are then easily completed, giving

$$\dot{n}_\pm \Big|_{\triangleright} = f_{\triangleright} n_{\text{GJ}} \frac{\sigma_{X\gamma}^0 \Theta_{\text{bb}} c}{\pi^2 \lambda_e^3} \int \frac{d\mathcal{M}_\gamma}{d\omega_\gamma} \Big|_{\triangleright} \left(\frac{c}{\lambda_e \omega_\gamma} \right)^2 \ln \left[1 - \exp \left(-\frac{2m_e c^2}{\hbar \omega_\gamma \Theta_{\text{bb}}} \right) \right] d\omega_\gamma, \quad (79)$$

where we have taken $\mu_{\text{min}} = 0$. The corresponding expression for the ingoing charges is

$$\dot{n}_\pm \Big|_{\triangleleft} = f_{\triangleleft} n_{\text{GJ}} \frac{\sigma_{X\gamma}^0 \Theta_{\text{bb}} c}{\pi^2 \lambda_e^3} \int \frac{d\mathcal{M}_\gamma}{d\omega_\gamma} \Big|_{\triangleleft} \left(\frac{c}{\lambda_e \omega_\gamma} \right)^2 \ln \left[\frac{1 - \exp(-2m_e c^2 / \hbar \omega_\gamma \Theta_{\text{bb}})}{1 - \exp(-m_e c^2 / \hbar \omega_\gamma \Theta_{\text{bb}})} \right] d\omega_\gamma. \quad (80)$$

To obtain the net pair creation rate per unit area of the gap, the multiplicity $d\mathcal{M}_\gamma/dE_\gamma$ of gamma rays created by resonant scattering must be weighted by the distance $\Delta z = h - z$ (z between the position z of resonant scattering and the outer (inner) boundary of the gap. The number of pairs that are spawned within the gap by each outgoing or ingoing charge is, then,

$$N_\pm \Big|_{\triangleright, \triangleleft} = \frac{1}{f_{\triangleright, \triangleleft} n_{\text{GJ}} c} \int d\omega_\gamma (h - \Delta z) \frac{d\dot{n}_\pm \Big|_{\triangleright, \triangleleft}}{d\omega_\gamma}. \quad (81)$$

Here Δz is the distance from the injection boundary. The relation between frequency and position within the gap is obtained by assuming that $\hbar\omega_\gamma = f_{\text{recoil}} \gamma(\Delta z) m_e c^2$, where $\gamma(\Delta z)$ is given by eq. (43), and the recoil factor f_{recoil} by eq. (55). The energy $\hbar\omega_{X,0}$ of the initial target X-ray is given by

$$\begin{aligned} \tilde{\omega}_\triangleright &= \frac{\hbar\omega_{X,0}}{k_B T_{\text{bb}}} = \frac{B/B_Q}{\gamma \Theta_{\text{bb}}} \\ &= \frac{f_{\text{recoil}}(B/B_Q)}{\Theta_{\text{bb}}} \left(\frac{\hbar\omega_\gamma}{m_e c^2} \right)^{-1}. \end{aligned} \quad (82)$$

This expression applies to an outgoing charge; similarly one has

$$\tilde{\omega}_\triangleleft = \frac{1}{2} \tilde{\omega}_\triangleright = \frac{f_{\text{recoil}}(B/B_Q)}{2\Theta_{\text{bb}}} \left(\frac{\hbar\omega_\gamma}{m_e c^2} \right)^{-1}. \quad (83)$$

for an ingoing charge. The integrals over ω_γ in eq. (79) and (80) can then be transformed to integrals over $\tilde{\omega}_\triangleright$ and $\tilde{\omega}_\triangleleft$. One finds,

$$N_\pm \Big|_{\triangleright, \triangleleft} = K_{X\gamma} \frac{h}{R_{\text{NS}}} I_{\triangleright, \triangleleft} \quad (84)$$

where

$$\begin{aligned} K_{X\gamma} &\equiv \frac{0.15 \alpha_f \Theta_{\text{bb}}^5}{\gamma_{\text{max}}^2 \mathcal{F}(B)} \left(f_{\text{recoil}} \frac{B}{B_Q} \right)^{-2} \left(\frac{\sigma_{X\gamma}^0 R_{\text{NS}} R_C}{\lambda_e^4} \right) \\ &= \frac{26 \mathcal{F}^{1/2}}{A^{1/2} f_{\text{recoil}}^2} \frac{R_{\text{NS},6}}{B_{\text{NS},14}^{5/2}} \left(\frac{\sigma_{X\gamma}^0}{0.02 \sigma_T} \right) \left(\frac{k_B T_{\text{bb}}}{0.5 \text{ keV}} \right)^5 \left(\frac{P}{6 \text{ s}} \right)^{1/2} \left(\frac{R_C}{R_{\text{NS}}} \right)^{-1/2}, \end{aligned} \quad (85)$$

and

$$\begin{aligned} I_\triangleright &\equiv \int_{\tilde{\omega}_{\triangleright, \text{min}}}^{\infty} d\tilde{\omega}_\triangleright \frac{\tilde{\omega}_\triangleright^2}{(\Delta z/h)} \ln(1 - e^{-\tilde{\omega}_\triangleright}) \ln \left[1 - e^{-2\tilde{\omega}_\triangleright / f_{\text{recoil}}(B/B_Q)} \right]; \\ I_\triangleleft &\equiv 8 \int_{\tilde{\omega}_{\triangleleft, \text{min}}}^{\infty} d\tilde{\omega}_\triangleleft \frac{\tilde{\omega}_\triangleleft^2}{(\Delta z/h)} \ln \left[\frac{1 - e^{-2\tilde{\omega}_\triangleleft}}{1 - e^{-\tilde{\omega}_\triangleleft}} \right] \ln \left[\frac{1 - e^{-4\tilde{\omega}_\triangleleft / f_{\text{recoil}}(B/B_Q)}}{1 - e^{-2\tilde{\omega}_\triangleleft / f_{\text{recoil}}(B/B_Q)}} \right]. \end{aligned}$$

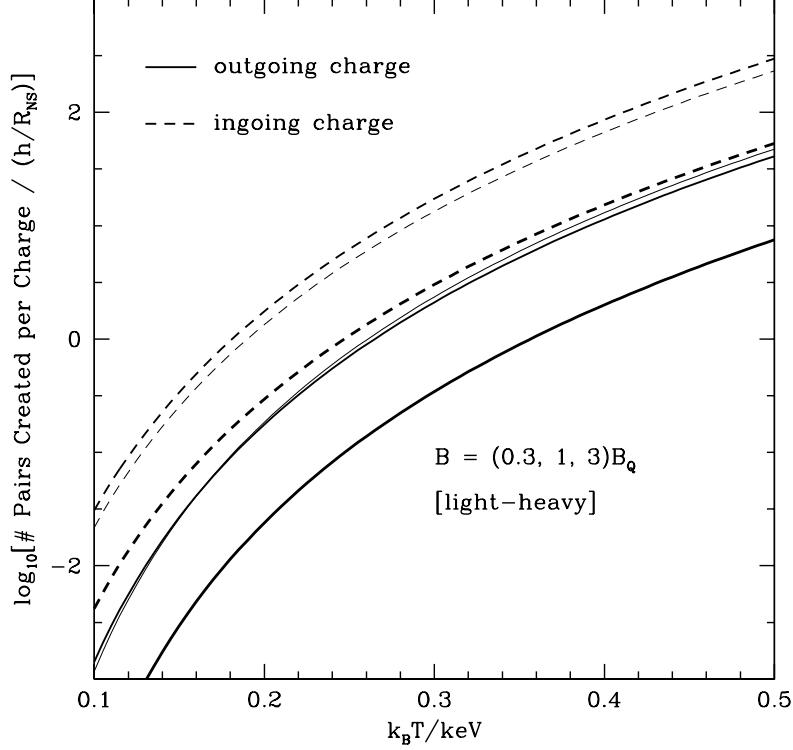


FIG. 9.— Number of pairs created per charge flowing through a surface gap, by collisions between thermal X-rays and resonantly scattered X-rays. The gap solution is given by eq. (22), with $B < 4B_Q$. The contributions from outgoing and ingoing charges are evaluated separately. The gap voltage is reduced by this process where eq. (87) is satisfied. Each set of three curves corresponds to magnetic fields $0.3B_Q$, B_Q and $3B_Q$ (thicker curves representing stronger fields). We choose parameters $A = 1$, $R_{NS} = 10$ km, $R_C = R_{NS}$ and $P = 6$ s.

(86)

The minimum values of $\tilde{\omega}_{\triangleright}$ and $\tilde{\omega}_{\triangleleft}$ are found by substituting $\gamma = \gamma_{\max}$ in eqs. (82), (83). The numbers of pairs that are spawned within the gap by outgoing and ingoing charges are plotted separately in Fig. 9. Note that we have extracted a factor of h/R_{NS} in the definition of $K_{X\gamma}$.

3.3.3. Reduction in the Gap Voltage

We now evaluate the effect of these secondary modes of pair creation on the gap structure. The voltage drops below the value given by eqs. (40) and (52) when the pair creation rate inside the gap is high enough that the inequality (62) is violated. Self-consistent values of the gap thickness and voltage can be obtained by summing the rates of pair creation due to nonresonant scattering (§3.3.1) and collisions of gamma-rays with thermal X-rays (§3.3.2), and then arbitrarily adjusting Φ_{gap} by a factor ε_{gap} . (The effect of resonant drag on the particle dynamics is neglected in calculating the pair creation rate.) A simple iteration gives a unique value of ε_{gap} at which the screening condition (62) is marginally satisfied. The Lorentz factor at a fixed fractional depth z/h in the gap scales as $\gamma \propto \varepsilon_{\text{gap}}$, and the thickness as $h \propto \varepsilon_{\text{gap}}^{1/3}$ (eq. [22]). The coefficient $K_{X\gamma}$ as defined in eq. (85) scales as $K_{X\gamma} \propto \varepsilon_{\text{gap}}^{-2}$.

When the gap is partially screened, its voltage depends on the the outgoing and ingoing particle densities $f_{\triangleright, \triangleleft} \times n_{GJ}$ (eq. [77]). The screening condition (62) is readily expressed in terms of the quantities $N_{\pm}|_{\triangleright, \triangleleft}$ and $f_{\triangleright, \triangleleft}$,

$$\frac{f_{\triangleright} N_{\pm}|_{\triangleright} + f_{\triangleleft} N_{\pm}|_{\triangleleft}}{h/R_{NS}} \lesssim \frac{A}{4}. \quad (87)$$

At the surface of the star, pair creation is mainly due to the ingoing charges when $f_{\triangleleft} = O(1)$. One expects that the gap voltage is only gradually reduced as the reverse inequality becomes satisfied: as the energy of the target X-rays is pushed further out onto the Wien tail, the number of targets drops exponentially.

This expectation is borne out in Fig. 10. There is a critical surface blackbody temperature of about 0.15-0.2 keV above which the gap voltage is reduced. In the case where $B_{NS} = 3B_Q$, there is a reduction of a factor 3 at $k_B T_{\text{bb}} = .23$ keV when $J = 1.5\rho_{GJC}$, and at $k_B T_{\text{bb}} = 0.26$ keV when $J = 1.1\rho_{GJC}$. A comparison of Figs. 8 and 9 shows that photon collisions are somewhat less efficient at making pairs than non-resonant scattering when B_{NS} is stronger than 10^{14} G, but are a much more important source of pairs

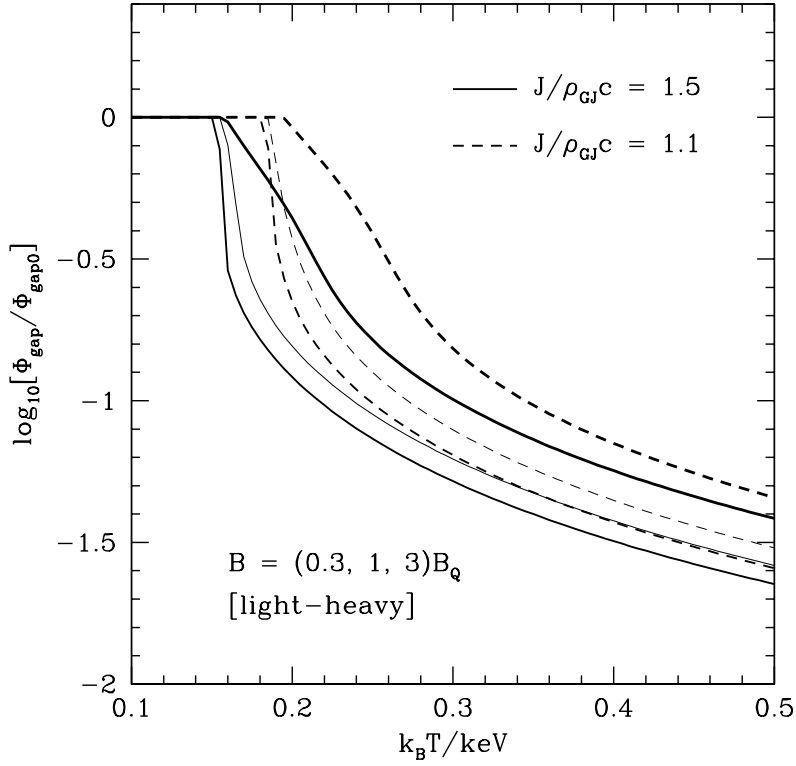


FIG. 10.— Reduction in the surface gap voltage Φ_{gap} due to pair creation inside the gap by non-resonant scattering of high energy X-rays, and collisions between gamma rays and thermal X-rays. The unscreened gap voltage $\Phi_{\text{gap}0}$ is given by eqs. (40) and (52). The result is given for various magnetic field strengths and for two values of $J/\rho_{\text{GJ}}c$.

when B_{NS} is close to B_{Q} and $k_{\text{B}}T_{\text{bb}}$ is larger than ~ 0.2 keV. The relative rates of pair creation by these two processes are plotted for a few values of B_{NS} in Fig. 11.

It should be noted that the total kinetic energy that is gained by the outgoing charges in crossing the gap, as given by eq. (52) with the correction of Fig. 10, is larger than the power radiated in gamma rays during their transit through the gap. As a result, most of the pair creation that is induced by the gap occurs *outside the gap*, where the primary charges are decelerated by resonant drag (§4.1).

4. CYCLOTRON DRAG ON THE SECONDARY PAIRS

4.1. Increase in Pair Multiplicity due to Continued Resonant Scattering

Pairs that are created close to the star will continue to scatter off ambient X-rays as they flow outward. The resonant drag force is stronger in more rapidly rotating neutron stars (e.g. young magnetars or young pulsars with high X-ray luminosities), and especially in magnetars with active, scattering magnetospheres. The flux of pairs can increase significantly through the conversion of the scattered X-rays, if the initial pairs are energetic enough. We neglect the possibility that the pairs are continuously reaccelerated, as they would be if the magnetic field were strongly turbulent (Lyutikov & Thompson 2005; Thompson 2008). The pair cascade then feeds off the initial kinetic energy of the outflowing charges, and additional generations of pairs can be created only within a limited distance from the star.

Detailed expressions for the drag force experienced by relativistic magnetized electrons in a radiation field can be found in Dermer (1990), who was interested in the application to gamma ray bursts. Kardashev et al. (1984), Sturmer (1995), and Lyubarskii & Petrova (1998) consider the interaction of outgoing particles with thermal photons near the polar cap of a neutron star, but do not consider the interaction further out in the magnetosphere, where the photon field is increasingly anisotropic.

We suppose that outgoing electrons and positrons are created with $\gamma_{\triangleright} \gtrsim \gamma_{\triangleright}^{\ominus}$ (eq. [34]) near the surface of the star. A charge will lose a significant fraction of its kinetic energy to resonant scattering over a distance $\sim r$ if

$$f_{\text{recoil}} \Gamma_{\triangleright}^{\text{res}} \frac{r}{c} \sim 1, \quad (88)$$

where $f_{\text{recoil}} \simeq B/B_{\text{Q}}$ in magnetic fields weaker than B_{Q} (eq. [55]). Evaluating expression for the scattering rate off a blackbody photon gas on the Wien tail of the distribution, one finds

$$\frac{e\tilde{\omega}_{\triangleright}}{\tilde{\omega}_{\triangleright}^2} = 9.8 \times 10^3 \frac{R_{\text{NS},6}}{B_{\text{NS},14}} \left(\frac{B}{B_{\text{Q}}} \right) \left(\frac{k_{\text{B}}T_{\text{bb}}}{0.5 \text{ keV}} \right)^3 \quad (89)$$

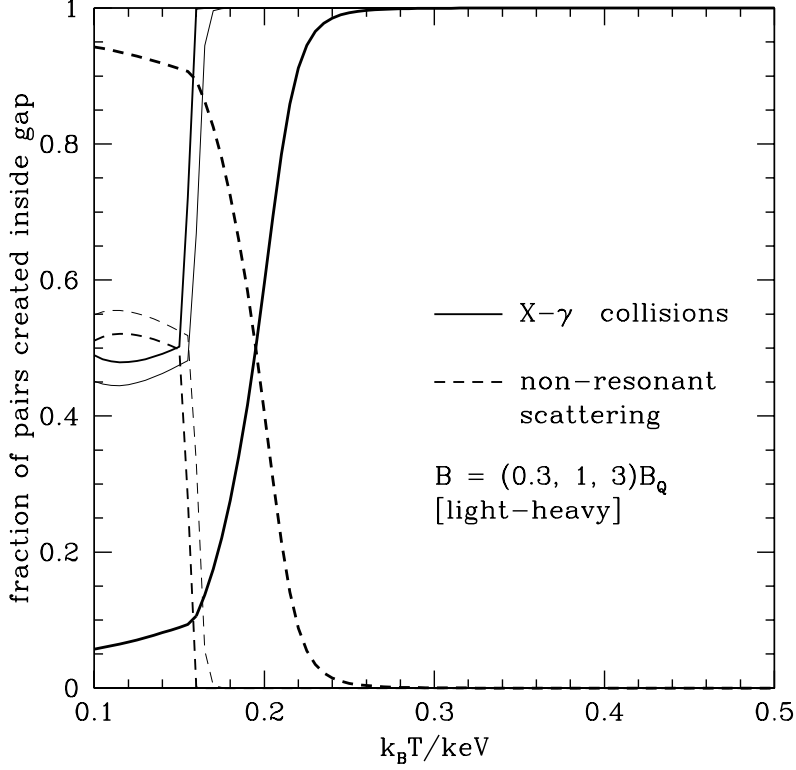


FIG. 11.— Proportions of the pair creation inside a surface gap due to the direct conversion of non-resonantly scattered X-rays off the magnetic field (§3.3.1), and to collisions between gamma rays and thermal X-rays (§3.3.2). The first process is more important at temperatures below 0.2–0.3 keV, and the second at higher temperatures. The current flowing through the gap is taken to be $J = 1.5 \rho_{\text{GI}} c$. The break in the curves at $k_B T_{\text{bb}} \sim 0.16$ keV occurs where partial screening first becomes effective.

where $\tilde{\omega}_{\triangleright} = \gamma_{\triangleright}^{\ominus} / \gamma_{\triangleright}$.

The resonantly scattered photons have an energy $E_{\gamma} \simeq \gamma_{\triangleright} (B/B_Q) m_e c^2$. They continue to convert to electron-positron pairs off the magnetic field as long as

$$E_{\gamma} \theta_{k_B} \simeq E_{\gamma} \frac{r}{R_C(r)} > 2m_e c^2. \quad (90)$$

The pair creation zone sits close enough to the star that we assume that the field curvature radius R_C is dominated by the quadrupole/octopole component of the magnetic field (eq. [A9]). Then the threshold condition (90) can be expressed as

$$\tilde{\omega}_{\triangleright} < \frac{\tilde{\varepsilon}_3}{\Theta_{\text{bb}}} \left(\frac{B}{B_Q} \right)^2. \quad (91)$$

We can now determine the limiting radius R_{\pm} for pair creation, and the characteristic energy of the outflowing particles at that radius. The value of $\tilde{\omega}_{\triangleright}$ deduced from eq. (89) varies from $\tilde{\omega}_{\triangleright} \simeq 10$ near the surface of the star to $\tilde{\omega}_{\triangleright} \simeq 7$ at the limiting radius for pair creation. The energy of the outgoing charges, as limited by drag, is

$$\gamma_{\triangleright}(\text{drag}) = \frac{B/B_Q}{\tilde{\omega}_{\triangleright} (1 - \mu_{\text{min}}) T_{\text{bb}}}, \quad (92)$$

and decreases from $\gamma_{\triangleright} \simeq 300 (B_{\text{NS}}/3B_Q) (k_B T_{\text{bb}}/0.5 \text{ keV})^{-1}$ at the surface of the star. The magnetic field at $r = R_{\pm}$ works out to

$$B_{\text{min}}(R_{\pm}) = 4.0 \times 10^{12} \tilde{\varepsilon}_3^{-1/2} \left(\frac{k_B T_{\text{bb}}}{0.5 \text{ keV}} \right)^{1/2} \text{ G}. \quad (93)$$

Hence $f_{\text{recoil}} \simeq B_{\text{min}}/B_Q \sim 0.1$, which means that the last generation of pairs that is created by the conversion of resonantly scattered photons is well separated in energy from the scattering charges. The characteristic energy of the latter has dropped to

$$\gamma_{\triangleright}(\text{drag}) = \frac{\gamma_{\triangleright}^{\ominus}}{\tilde{\omega}_{\triangleright}} = \frac{B_{\text{min}}/B_Q}{\tilde{\omega}_{\triangleright} (1 - \mu_{\text{min}}) \Theta_{\text{bb}}}$$

$$= 2 \times 10^2 \tilde{\varepsilon}_3^{-1/6} B_{\text{NS},14}^{2/3} \left(\frac{k_B T_{\text{bb}}}{0.5 \text{ keV}} \right)^{-5/6} \quad (r = R_{\pm}), \quad (94)$$

and the secondary pairs have an energy

$$\begin{aligned} \gamma_{\triangleright}[2] &= \frac{E_\gamma}{2m_e c^2} = \left(\frac{B_{\text{min}}}{2B_Q} \right) \gamma_{\triangleright}(\text{drag}) \\ &= 10 \tilde{\varepsilon}_3^{-2/3} B_{\text{NS},14}^{2/3} \left(\frac{k_B T_{\text{bb}}}{0.5 \text{ keV}} \right)^{-1/3} \quad (r = R_{\pm}). \end{aligned} \quad (95)$$

The primary outflowing charges are injected with an energy $\gamma_0 \sim 10^3 - 10^4$ in the gap model described above. In this case, the outflowing charges multiply rapidly just outside the gap. Their energy spectrum can be derived as follows (again assuming negligible reacceleration). The mean number of photons scattered in a radial interval dr is $dN_\gamma = \Gamma_{\triangleright}^{\text{res}} dr/c$, and the loss of energy due to scattering is $d\gamma = (f_{\text{recoil}} \gamma) \Gamma_{\triangleright}^{\text{res}} dr/c$. Focusing on the zone where $B \lesssim B_Q$, and the gamma ray carries off a small fraction of the kinetic energy of the scattering charge, the energy spectrum of the gamma rays and created pairs can be written as

$$\gamma_{\triangleright}[2] \frac{dN_{\pm}}{d\gamma[2]} = E_\gamma \frac{dN_\gamma}{dE_\gamma} = \left\{ \frac{d[f_{\text{recoil}} \gamma_{\triangleright}(\text{drag})]}{d\gamma_{\triangleright}(\text{drag})} \right\}^{-1}. \quad (96)$$

Since $\gamma_{\triangleright}(\text{drag})$ scales approximately as $\sim r^{-1}$, and $B(r) \propto r^{-3}$, this gives the asymptotic formula

$$\gamma_{\triangleright}[2] \frac{dN}{d\gamma[2]} \simeq \frac{4}{B/B_Q} \quad (B \ll B_Q). \quad (97)$$

Most of the pairs are created near the limiting radius R_{\pm} , where the multiplicity of pairs per primary outgoing charge has increased to

$$\frac{\mathcal{M}_{\pm}}{\mathcal{M}_{\pm}|_{R_{\text{NS}}}} \simeq \frac{\gamma_0}{2\gamma_{\triangleright}[2]} = 500 \tilde{\varepsilon}_3^{2/3} B_{\text{NS},14}^{-2/3} \left(\frac{k_B T_{\text{bb}}}{0.5 \text{ keV}} \right)^{1/3} \left(\frac{\gamma_0}{10^4} \right). \quad (98)$$

A beam instability will, in fact, be triggered in this outflowing plasma, since the distribution of particle kinetic energy extends to relatively low values. The effect on the particle energy spectrum will be strongest in the outer part of the pair creation zone, where $f_{\text{recoil}} \ll 1$. A calculation of the energy spectrum including the combined effects of resonant drag and the beam instability has never been carried out, but would be very useful.

4.2. Limiting angle for Relativistic Pair Flows

In this section, we make a brief detour to address the effects of resonant drag in two cases: i) the neutron star has a relatively high X-ray luminosity ($L_X \gtrsim 10^{34}$ ergs s^{-1}) and a faster spin than the known magnetars ($P < 0.3$ s); and ii) a significant fraction of the thermal X-rays are backscattered from the magnetosphere by current-carrying charges.

The strength and sign of the drag force acting on the outgoing charges depends on the angle θ_{kB} between their motion along \mathbf{B} , and the target photons. The thermal radiation emitted from the surface of the neutron star becomes increasingly collimated at greater distances; but at the same time the open dipolar⁶ field lines become more strongly curved. The maximum angle value of θ_{kB} at the end of the open-field bundle is given by

$$1 - \mu_{\text{min}} = \frac{1}{2} \max \left(\frac{R_{\text{NS}}^2}{r^2}, \frac{\Omega r}{4c} \right). \quad (99)$$

The first term is the large-radius expansion of eq. (31). The collimation of the target photons about the local direction of the magnetic field is tightest at a radius (Fig. 12)

$$R_{\text{col}} = \left(\frac{4c}{\Omega R_{\text{NS}}} \right)^{1/3} R_{\text{NS}} = 12.4 R_{\text{NS},6}^{-1/3} \left(\frac{P}{0.1 \text{ s}} \right)^{1/3} R_{\text{NS}}. \quad (100)$$

Expression (32) for the scattering rate $\Gamma_{\triangleright}^{\text{res}}$ of the outgoing charges is modified at $r > R_{\text{col}}$. One replaces

$$(1 - \mu_{\text{min}})^2 \rightarrow \left(\frac{R_{\text{NS}}^2}{2r^2} \right) \left(\frac{\Omega r}{8c} \right). \quad (101)$$

The first factor represents the continuing dilution of the target radiation field as it flows away from the surface of the star, and the second represents the factor $1 - \mu$ in the scattering rate. The fraction of the particle momentum lost to drag is given by

$$f_{\text{recoil}} \Gamma_{\triangleright}^{\text{res}} \frac{r}{c} = \frac{\alpha_f \Theta_{\text{bb}}^3}{32} \left(\frac{\Omega R_{\text{NS}}}{c} \right) \left(\frac{R_{\text{NS}}}{\lambda_e} \right) \tilde{\omega}_{\triangleright}^2 e^{-\tilde{\omega}_{\triangleright}} \quad (\theta = \theta_{\text{open}}). \quad (102)$$

⁶ We consider the effect of higher multipoles only when evaluating the threshold energy for single-photon pair creation at $r < R_{\text{col}}$.

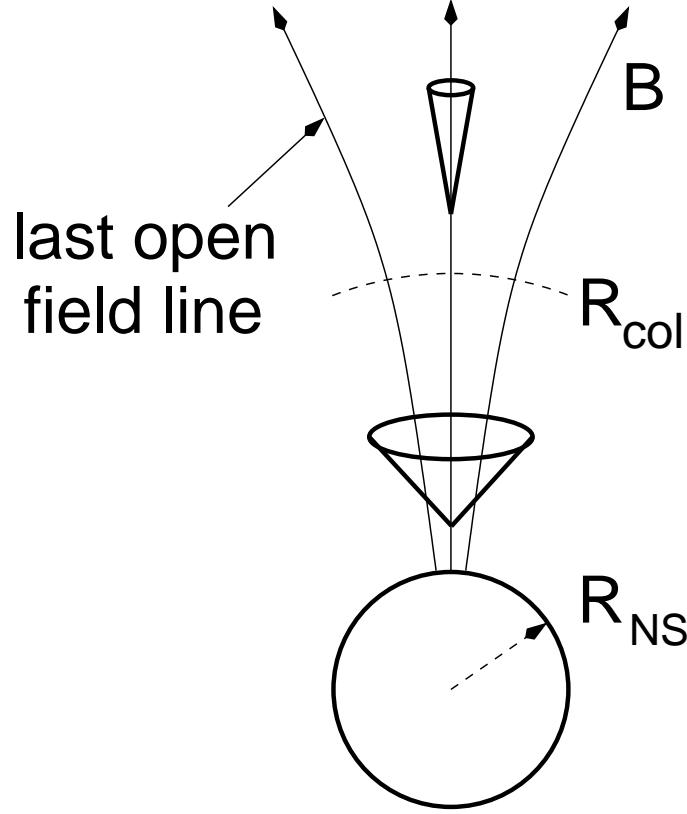


FIG. 12.— Close to the neutron star, the thermal X-rays emitted from its surface fill a wide cone. Beyond a distance R_{col} (eq. [100]), the angle between the propagation direction of a photon and the open magnetic field lines is dominated by the field-line curvature.

Note that the coefficient is independent of radius. If the spin of the star is fast enough, then the right-hand side of eq. (102) can exceed unity – not only at $r \sim R_{\text{col}}$, but out to a very large distance from the star. The right-hand side is maximized at $\tilde{\omega}_{\triangleright} = 2$, and is greater than unity if

$$P < 0.4 R_{\text{NS},6}^{1/2} \left(\frac{L_X^\infty}{10^{35} \text{ ergs s}^{-1}} \right)^{3/4}. \quad (103)$$

This defines the critical spin period below which the motion of the secondary pairs is strongly reduced by resonant scattering at $\theta \sim \theta_{\text{open}}$.

On a closed field line that is anchored at a polar angle $\theta(R_{\text{NS}}) > (\Omega R_{\text{NS}}/c)^{1/2}$, expression (102) generalizes to

$$f_{\text{recoil}} \Gamma_{\triangleright}^{\text{res}} \frac{r}{c} = \frac{\alpha_f \Theta_{\text{bb}}^3}{32} \theta^2(R_{\text{NS}}) \left(\frac{R_{\text{NS}}}{\lambda_e} \right) \tilde{\omega}_{\triangleright}^2 e^{-\tilde{\omega}_{\triangleright}}. \quad (104)$$

Charges moving through the closed magnetosphere will experience strong drag if the guiding magnetic field lines are anchored at an angle larger than

$$\theta_{\text{max}}(R_{\text{NS}}) = 1.36 R_{\text{NS},6}^{1/2} \left(\frac{L_X^\infty}{10^{35} \text{ ergs s}^{-1}} \right)^{-3/8} \text{ deg.} \quad (105)$$

4.2.1. Young Magnetars and Neutron Stars with Fast Spins and Large X-ray Luminosities

Let us now consider the limiting Lorentz factor of the outgoing secondary pairs when cyclotron drag is strong at $r > R_{\text{col}}$. We focus here on the open magnetic field lines, and therefore on stars which are spinning faster than the known magnetars, with periods smaller than (103). The force on a scattering charge vanishes when its Lorentz factor $\gamma = 1/\sin \theta_{kB}$. The equilibrium value is

$$\gamma_{\text{eq}} \simeq 2 \left(\frac{c}{\Omega r} \right)^{1/2} = 12.4 \left(\frac{P}{0.1 \text{ s}} \right)^{1/3} \left(\frac{r}{R_{\text{col}}} \right)^{-1/2} \quad (r > R_{\text{col}}) \quad (106)$$

when the cyclotron scattering rate is very high. We can compare eq. (106) with the Lorentz factor which the scattering rate of an outgoing charge is maximum,

$$\begin{aligned}\gamma_{\triangleright}^p &= \frac{\gamma_{\triangleright}^{\Theta}}{2} = \frac{B/B_Q}{2(1-\mu_{\min})\Theta_{\text{bb}}} \\ &= 2.2 \times 10^2 B_{\text{NS},14} R_{\text{NS},6}^{1/3} \left(\frac{P}{0.1 \text{ s}} \right)^{-1/3} \left(\frac{L_X^{\infty}}{10^{35} \text{ ergs s}^{-1}} \right)^{-1/4} \left(\frac{r}{R_{\text{col}}} \right)^{-4} \quad (r > R_{\text{col}}).\end{aligned}\quad (107)$$

One has $\gamma_{\triangleright}^p > \gamma_{\text{eq}}$ at $r = R_{\text{col}}$, so that resonant scattering decelerates an outgoing charge at this radius. The equilibrium Lorentz factor is attained a bit further from the star, at the radius

$$\frac{R_{\text{eq}}}{R_{\text{col}}} = 2.3 B_{\text{NS},14}^{2/7} R_{\text{NS},6}^{4/21} \left(\frac{P}{0.1 \text{ s}} \right)^{-4/21} \left(\frac{L_X^{\infty}}{10^{35} \text{ ergs s}^{-1}} \right)^{-1/14} \quad (108)$$

where

$$\gamma_{\text{eq}} = \gamma_{\triangleright}^p = 8.3 B_{\text{NS},14}^{-1/7} R_{\text{NS},6}^{-3/7} \left(\frac{P}{0.1 \text{ s}} \right)^{3/7} \left(\frac{L_X^{\infty}}{10^{35} \text{ ergs s}^{-1}} \right)^{1/28}. \quad (109)$$

A charge is able to maintain $\gamma \simeq \gamma_{\text{eq}}$ only over a modest range in radius. It continues to scatter off the Rayleigh-Jeans tail of the spectrum, and then decouples from the radiation field where the resonant frequency is $\tilde{\omega}_{\triangleright}^{\infty} \lesssim 1$, and the asymptotic Lorentz factor is

$$\gamma_{\infty} = \left(\frac{\tilde{\omega}_{\triangleright}^{\infty}}{2} \right)^{1/7} \gamma_{\text{eq}}(R_{\text{eq}}) \sim (0.7-0.9) \gamma_{\text{eq}}(R_{\text{eq}}). \quad (110)$$

We reach an interesting conclusion: the outflowing charges are decelerated to a small Lorentz factor γ_{∞} at a distance 20–30 R_{NS} from the star when the spin period is shorter than the value (103). Unless the secondary charges are reaccelerated farther out in the magnetosphere, the radio emission will experience a high optical depth to induced scattering; and there would be a bias against detecting pulsed radio emission from neutron stars with high X-ray luminosities and short spin periods.

4.2.2. Effects of Photons Scattered in the Closed Magnetosphere of a Magnetar

The scattering of thermal X-ray photons by trans-relativistic charges in the closed magnetosphere creates a second component of the radiation field, which is weaker but much more isotropic (Thompson et al. 2002). Photons from near the thermal peak are scattered at a radius

$$R_{\text{res}} \simeq \left(\frac{eB_{\text{NS}}}{m_e c \omega_X} \right)^{1/3} = 23 B_{\text{NS},15}^{1/3} \left(\frac{\hbar \omega_X}{\text{keV}} \right)^{-1/3} R_{\text{NS}}. \quad (111)$$

This scattered radiation field can exert a strong drag force on outgoing charges. We derive an upper bound on its intensity, if the outflowing secondary charges are to avoid being decelerated to trans-relativistic speeds.

The scattered X-rays subtend a wide range of angles, which means that they can resonate with the outflowing charges at a relatively small radius. Most of the drag force is supplied by photons from the black body peak, and so we approximate the spectral intensity of the scattered radiation as

$$4\pi I_{\omega} \simeq \left(\frac{\tau_{\text{res}}}{2} \right) \frac{L_X}{4\pi R_{\text{res}}^2(\omega_{\text{bb}})} \delta(\omega - \omega_{\text{bb}}), \quad (112)$$

where $\omega_{\text{bb}} \sim 1 \text{ keV}$ in the case of an X-ray bright magnetar.

The drag force in the rest frame of a charge moving parallel to \mathbf{B} is

$$F'_{\parallel} = \int d\omega' 2\pi \int_{\mu'_{\min}}^1 \frac{\mu' I_{\omega'}}{c} \sigma_{\text{res}}(\omega') d\mu', \quad (113)$$

where the scattering cross section at the cyclotron resonance is given by⁷ eq. (30). Transforming to the frame of the star gives $\mu' I_{\omega'} d\mu' = \gamma(\mu - \beta_e) I_{\omega} d\mu$, and

$$F_{\parallel} = F'_{\parallel} = \gamma \frac{4\pi^3 e^2}{m_e c^2} \int_{\mu_{\min}}^1 d\mu (\mu - \beta_e) I_{\omega}. \quad (114)$$

Substituting expression (112) into this integral gives the drag time $t_{\text{drag}} = \gamma m_e c / |F_{\parallel}|$,

$$\frac{ct_{\text{drag}}(r)}{r} = \left(\frac{\gamma^2}{\tau_{\text{res}}} \right) \frac{64\omega_{\text{bb}}^3 R_{\text{res}}^2(\omega_{\text{bb}}) m_e^2 c^2}{3\sigma_T B^2 L_X r} \quad (115)$$

⁷ Here we assume that the charge is moving relativistically, so that the photons are nearly collimated with \mathbf{B} in its rest frame.

The scattered photons which resonate with the newly created pairs propagate in the direction

$$1 - \mu = \frac{eB}{\gamma m_e c \omega_{\text{bb}}}, \quad (116)$$

and there is a maximum magnetic field for which a resonant interaction is possible (corresponding to $\mu \simeq 0$),

$$B_{\text{max}} = 8.6 \times 10^{12} \left(\frac{\gamma}{10^2} \right) \left(\frac{\hbar \omega_{\text{bb}}}{\text{keV}} \right) \text{ G}. \quad (117)$$

The drag force (115) at $B < B_{\text{max}}$ is

$$\frac{c t_{\text{drag}}(r)}{r} = 0.012 \tau_{\text{res}}^{-1} \frac{B_{\text{NS},15}^{1/3} R_{\text{NS},6}}{L_{X,35}} \left(\frac{\gamma}{10^2} \right)^{1/3} \left(\frac{\hbar \omega_{\text{bb}}}{\text{keV}} \right)^{2/3} \left(\frac{B}{B_{\text{max}}} \right)^{-5/3}, \quad (118)$$

and depends weakly on γ . The resonating photons comprise a fraction $\sim \frac{1}{2}(1 - \mu)$ of the backscattered flux. The secondary pairs slow down unless $\tau_{\text{res}} L_X \lesssim 10^{33} \text{ ergs s}^{-1}$.

5. LOW-VOLTAGE CIRCUIT WITH PAIRS SUPPLIED BY RESONANT SCATTERING

We now turn to the case where the polar magnetic field of the neutron star is stronger than $4B_Q = 1.8 \times 10^{14} \text{ G}$. Close to the surface, a significant fraction of resonantly scattered photons are above threshold for conversion to an electron-positron pair. The distance $\Delta z'$ for the conversion of a gamma ray to a pair is therefore very small. The net effect on the surface gap structure is to take $R_C \rightarrow 0$ in eq. (46), so that its thickness (51) and voltage (52) are forced to zero.

We therefore consider the alternative circuit model, with a lower voltage, that was outlined in §2.1. In this model, pair creation is smoothly distributed throughout the circuit, in such a way as to compensate the gradient in corotation charge density. The resonant scattering of X-rays from the exponential tail of the blackbody distribution can easily provide enough pairs: if the charges flowing through the circuit were energetic enough to scatter thermal X-rays from the black body peak, then the mean free path to scattering would be very small, $c/\Gamma_{\text{res}} r \sim 10^{-2} - 10^{-3}$ from eq. (35).

The pair creation rate per unit volume is

$$\dot{n}_{\pm} \simeq n_{\triangleright} \Gamma_{\triangleright}^{\text{res}} + n_{\triangleleft} \Gamma_{\triangleleft}^{\text{res}} \quad (119)$$

in the zone where $B > 4B_Q$. As before, n_{\triangleright} and n_{\triangleleft} are the number densities of ingoing and outgoing charges, and $\Gamma_{\triangleright}^{\text{res}}$, $\Gamma_{\triangleleft}^{\text{res}}$ are the respective rates of resonant scattering as given by eqs. (32), (36). Substituting for \dot{n}_{\pm} from eq. (13), we find

$$\Gamma_{\triangleright}^{\text{res}} \frac{n_{\triangleright}}{n_{\text{GJ}}} + \Gamma_{\triangleleft}^{\text{res}} \frac{n_{\triangleleft}}{n_{\text{GJ}}} \simeq \frac{c}{2} \frac{d \ln \dot{N}_{\text{GJ}}}{dr}. \quad (120)$$

We further have $\Gamma_{\triangleright}^{\text{res}} \propto e^{-\tilde{\omega}_{\triangleright}}/\gamma_{\triangleright}^2$ and $\Gamma_{\triangleleft}^{\text{res}} \propto e^{-\tilde{\omega}_{\triangleleft}}/\gamma_{\triangleleft}^2$. The characteristic dimensionless frequencies $\tilde{\omega}_{\triangleright}$ and $\tilde{\omega}_{\triangleleft}$ of the target photons are given by eqs. (33) and (38), and are related by

$$\tilde{\omega}_{\triangleright} = \frac{1 - \mu_{\text{min}}}{2} \tilde{\omega}_{\triangleleft}. \quad (121)$$

In other words, an outgoing charge must attain a higher energy to scatter a photon of a given frequency than does an ingoing charge. This difference in resonant energy grows with radius. For a target photon of energy $\hbar \omega_X = k_B T_{\text{bb}}$, it is

$$\gamma_{\triangleright}^{\ominus} = \frac{B/B_Q}{\Theta_{\text{bb}}(1 - \mu_{\text{min}})} \simeq 1.6 \times 10^4 B_{\text{NS},15}^{2/3} \left(\frac{B}{B_Q} \right)^{1/3} \left(\frac{k_B T_{\text{bb}}}{0.5 \text{ keV}} \right)^{-1}, \quad (122)$$

versus

$$\gamma_{\triangleleft}^{\ominus} = \frac{B/B_Q}{2\Theta_{\text{bb}}} \simeq 5 \times 10^2 \left(\frac{B}{B_Q} \right) \left(\frac{k_B T_{\text{bb}}}{0.5 \text{ keV}} \right)^{-1}, \quad (123)$$

at $r \gg R_{\text{NS}}$.

Only a fraction of the outgoing and ingoing charges must scatter in order to satisfy eq. (120), which means that resonant drag has a small effect on the particle energies in this circuit model. The outgoing and ingoing charges pass through comparable potential drops and therefore have comparable energies, $\gamma_{\triangleright} \sim \gamma_{\triangleleft}$. We deduce that $\Gamma_{\triangleleft}^{\text{res}} \gg \Gamma_{\triangleright}^{\text{res}}$ because $\tilde{\omega}_{\triangleright} > 2\tilde{\omega}_{\triangleleft}$ and the scattering occurs on the exponential tail of the Planckian distribution. Equation (120) then simplifies to

$$2I_{\triangleleft} \Gamma_{\triangleleft}^{\text{res}} = c \frac{dI_{\text{GJ}}}{dr}. \quad (124)$$

The right-hand side of this equation can be written as $cI_{\text{GJ}} d \ln(\rho_{\text{GJ}}/B)/dr = AI_{\text{GJ}}c/r$, where the coefficient A (eq. [20]) includes the effects of relativistic frame dragging and magnetic field line curvature. The current carried by the ingoing charges in this circuit solution is given by eq. (16). The number of photons scattered per logarithm of radius works out to

$$\frac{\Gamma_{\triangleleft}^{\text{res}} r}{c} = \frac{dI_{\text{GJ}}/d \ln r}{I - I_{\text{GJ}}} = A \left(\frac{I}{I_{\text{GJ}}} - 1 \right)^{-1}. \quad (125)$$

One of the charges in each created pair will typically be decelerated by the electric field and reverse direction before it can scatter another X-ray. Our toy model for the circuit assumes that this reversal is instantaneous, i.e. it occurs within a small distance of the point of creation.

Substituting equation (36) for $\Gamma_{\triangleleft}^{\text{res}}$ in equation (125), and taking into account that $\tilde{\omega}_{\triangleleft} \gg 1$, i.e. the resonance X-rays are in the far exponential tail of the Planck spectrum, we get the equation for γ_{\triangleleft} ,

$$\frac{1}{\gamma_{\triangleleft}^2} \frac{\alpha_f \Theta_{\text{bb}} r}{2\lambda_e} \left(\frac{B}{B_Q} \right) \exp\left(-\frac{B/B_Q}{2\gamma_{\triangleleft} \Theta_{\text{bb}}}\right) = A \left(\frac{I}{I_{\text{GJ}}} - 1 \right)^{-1}. \quad (126)$$

For typical magnetar temperatures, $k_B T_{\text{bb}} \sim 0.5$ keV ($\Theta_{\text{bb}} \sim 10^{-3}$), the solution of equation (126) is well approximated by

$$\gamma_{\triangleleft} \simeq 800 B_{15} \left(\frac{k_B T_{\text{bb}}}{0.5 \text{ keV}} \right)^{-1}. \quad (127)$$

This corresponds to $\tilde{\omega}_{\triangleleft} \sim 15$, and the scattering occurs in the exponential tail of the black body distribution, as expected. As the ingoing particles move to smaller radii, γ_{\triangleleft} increases in proportion to $B \propto r^{-3}$. This acceleration is sustained by an electric field E_{\parallel} . The equation of motion for ingoing particles reads

$$-m_e c^2 \frac{d\gamma_{\triangleleft}}{dr} = eE_{\parallel} \quad (128)$$

Then we find

$$eE_{\parallel} \simeq \frac{3\gamma_{\triangleleft} m_e c^2}{r}. \quad (129)$$

The voltage distribution is found by integrating equation (129),

$$-e\Phi(r) = \int_{R_{\text{NS}}}^r eE_{\parallel} dr \simeq 800 m_e c^2 B_{\text{NS},15} \left(\frac{k_B T_{\text{bb}}}{0.5 \text{ keV}} \right)^{-1} \left[1 - \left(\frac{r}{R_{\text{NS}}} \right)^{-3} \right]. \quad (130)$$

The net potential drop between the surface of the neutron star and the surface $B = 4B_Q$ is of the order of $1 B_{\text{NS},15}$ GeV. If the primary outgoing particles are electrons ($\rho_{\text{GJ}} < 0$), they are accelerated to the Lorentz factor,

$$\gamma_{\triangleright}(r) \simeq -\frac{e\Phi(r)}{m_e c^2}. \quad (131)$$

The outgoing particles undergo negligible scattering, and contribute little to the net rate of pair creation, since they see target photons that are a factor $\simeq 2$ higher in frequency than do the ingoing charges. We therefore expect that this circuit solution should apply in the inner zone for either sign of ρ_{GJ} .

The voltage (130) can be compared with the gap solution (52), as reduced by secondary pair creation processes (Fig. 10). Normalizing the gap voltage to the threshold magnetic field $B_{\text{NS}} = 4B_Q$, we find

$$\frac{\Phi(r \gg R_{\text{NS}})}{\Phi_{\text{gap}}(B_{\text{NS}} = 4B_Q)} \simeq \left(\frac{B_{\text{NS}}}{4B_Q} \right) \left(\frac{\tilde{\varepsilon}_3}{0.3} \right)^{1/2} \left(\frac{P}{6 \text{ s}} \right)^{1/4} \times \begin{cases} 0.05 & (k_B T_{\text{bb}} = 0.1 \text{ keV}); \\ 0.1 & (k_B T_{\text{bb}} = 0.4 \text{ keV}). \end{cases} \quad (132)$$

Seeds for the ingoing e^{\pm} discharge are supplied from the zone where $B < 4B_Q$, and where voltage fluctuations are likely to be larger than they are in the inner circuit. In fact, the true solution in both zones may be time-dependent, with repeating avalanches of pair creation, as is seen in a one-dimensional model of the closed corona (Beloborodov & Thompson 2007). The main features of the steady circuit model should, however, survive in the time-dependent case: the ingoing particles dominate the rate of pair creation in the inner zone, that is, the pair avalanche is directed toward the star, and the time-averaged voltage is comparable to 1 GeV.

5.1. Stability of Voltage Solution I

We explained in the preceding section why the surface gap described in §3 cannot be maintained when $B_{\text{NS}} > 4B_Q$. We now address the stability question from the opposing angle: when $B_{\text{NS}} < 4B_Q$, does a gap spontaneously form in a circuit that is set up in the low-voltage solution, with smoothly distributed pair creation? We approach this question here by considering the stability of electrostatic modes in the circuit, but note that other degrees of freedom could be involved. In particular, a high-frequency current fluctuation would be generated by a turbulent cascade if the magnetic twist received a low frequency perturbation of a moderate amplitude (Lyutikov & Thompson 2005; Thompson 2008).

The instability in question bears some resemblance to the formation of a double layer within a current-carrying plasma. In an electron-ion plasma, such a structure is believed to be seeded by a two-stream instability, such as an ion-acoustic instability, which is driven by the drift motion of the electrons that supplies the current. Localized wavepackets that are formed via this instability undergo non-linear growth, leading to the formation of plasma holes which are bounded by layers of positive and negative charge. Multiple double layers can form within a single circuit, as is observed in the Earth's magnetosphere. A diode structure with a deeper potential drop may form through the coalescence a large number of weak double layers.

The low-voltage circuit consists of counterstreaming clouds of electrons and positrons, and so we first review what is known about the non-linear evolution of the two stream instability in a strongly magnetized pair plasma. Near the surface of a neutron star, the electron cyclotron frequency is many orders of magnitude larger than the plasma frequency, and so filamentation instabilities are suppressed. Guidance about the behavior of the two-stream instability can therefore be provided by one-dimensional simulations of the purely electrostatic instability. The perturbation will, in practice, have an electromagnetic component because plasma oscillations on different field lines have different phases.

We imagine preparing the ingoing and outgoing charges with a distribution function concentrated at momenta $p_{\parallel} = \pm \bar{\gamma} \bar{V} m_e$ parallel to \mathbf{B} . For simplicity, we focus on the case where $\rho_{\text{GJ}} \rightarrow 0$ (e.g. the open flux tube is anchored near the rotational equator). Then the plasma frequencies of the electrons and positrons are equal, and are given by

$$\omega_P^2 = \frac{4\pi n_{e^-}}{m_e} = \frac{4\pi n_{e^+}}{m_e} = \frac{2\pi J e}{m_e c}, \quad (133)$$

where the densities refer to the frame of the star. The dispersion relation is obtained from the longitudinal part of the dispersion tensor,

$$1 - \frac{\omega_P^2}{\bar{\gamma}^3(\omega + k\bar{V})^2} - \frac{\omega_P^2}{\bar{\gamma}^3(\omega - k\bar{V})^2} = 0. \quad (134)$$

The fastest growing mode has a growth rate and wavenumber

$$\Gamma_* = \frac{\omega_P}{2\bar{\gamma}^{3/2}}; \quad k_* = 3^{1/2} \frac{\Gamma_*}{\bar{V}}, \quad (135)$$

and a vanishing real frequency. Purely growing modes exist within the range of wavenumbers $k_* < k < 2^{3/2} \Gamma_* / \bar{V} = 1.6 k_*$. In practice, there is an imbalance in the densities of positive and negative charges, so that the growing modes have real frequencies of the order of Γ_* and finite phase speeds $V_{\text{ph}} \simeq c$.

Simulations of colliding relativistic plasma clouds in one dimension⁸ (e.g. Dieckmann 2005, Dieckmann et al. 2006) show the growth of electrostatic modes with a modest range of k centered on k_* , which then develop into a broad spectrum of electrostatic turbulence on a timescale $\simeq 50 \Gamma_*^{-1}$. A necessary condition for the existence of a beam-driven mode is, therefore,

$$50 \frac{V_{\text{ph}}}{\Gamma_*} \lesssim R_{\text{NS}}, \quad (136)$$

or equivalently

$$\bar{\gamma} \lesssim \left(10^{-2} \frac{\omega_P R_{\text{NS}}}{c} \right)^{2/3} = 7 \times 10^2 B_{\text{NS},14}^{1/3} R_{\text{NS},6}^{2/3} \left(\frac{P}{6 \text{ s}} \right)^{-1/3} \left(\frac{J}{\rho_{\text{GJ}} c} \right)^{1/3}. \quad (137)$$

Comparing this expression with eq. (127) for the equilibrium Lorentz factor $\gamma_{\triangleleft} = 80 B_{\text{NS},14} (k_{\text{B}} T_{\text{bb}} / 0.5 \text{ keV})^{-1}$ of the pair-creating charges (eq. [127]), one sees that this inequality is easily satisfied. Note that the growth of the beam-driven mode is not suppressed by the radial inhomogeneity of the pair plasma, because growing modes exist over a relatively broad range of wavenumbers.

A similar inequality can be obtained by supposing that the distribution function is flat at small momenta, so that the average of γ^{-3} over the distribution function is dominated by a small fraction $\sim 1/\bar{\gamma}$ of particles with momenta $p_{\parallel} \sim \pm m_e c$, $\langle \gamma^{-3} \rangle^{1/2} \sim 1/\bar{\gamma}^{1/2}$. A transrelativistic particle propagating through the background electric field gains energy at the rate $\gamma^{-1} d\gamma/dt \sim \bar{\gamma} c / R_{\text{NS}}$, which when equated with the growth rate (135) gives the same dependence on $\bar{\gamma}$ as in eq. (136).

The rate of pair creation changes in response to the beam-driven mode, and screening of E_{\parallel} by the pairs can suppress growth. We imagine that gamma rays are emitted and converted to free pairs, and that one of the particles so created immediately reverses direction in the background electric field. There is a critical value of the total free path for this process, denoted by Δz , below which the screening effect is important,

$$\Delta z < k_*^{-1} \sim \bar{\gamma}^{3/2} \frac{c}{\omega_P} = 0.5 \frac{\bar{\gamma}^{3/2}}{B_{\text{NS},14}^{1/2}} \left(\frac{P}{6 \text{ s}} \right)^{1/2} \text{ cm}. \quad (138)$$

When this inequality is violated, the gamma rays that are emitted within a localized potential perturbation convert to pairs at distant points in the circuit, where they cannot influence the growth of the potential. The minimal rate of pair creation needed to screen the growing, beam-driven potential fluctuation $\delta\Phi$ before a broad spectrum of electrostatic turbulence develops is

$$e \delta \dot{n}_{\pm} > \frac{1}{50} \Gamma_* \delta \rho. \quad (139)$$

Here

$$\delta \rho = \frac{k_*^2 \delta \Phi}{4\pi}, \quad (140)$$

⁸ These simulations are of two colliding electron-ion clouds, in which the ions supply a positive neutralizing charge distribution and do not strongly influence the growth of the instability.

is the corresponding charge density fluctuation. The change in the rate of gamma-ray emission per unit volume resulting from a potential fluctuation $\delta\Phi$ is given by

$$\delta\dot{n}_\gamma = \frac{\partial\dot{n}_\gamma}{\partial\bar{\gamma}} \frac{e\delta\Phi}{m_e c^2}. \quad (141)$$

If inequality (138) is satisfied, then $\delta\dot{n}_\pm \sim \delta\dot{n}_\gamma$, and we have a second condition for effective screening

$$k_* < \left(10^2 \frac{4\pi e^2}{m_e c^3} \frac{\partial\dot{n}_\pm}{\partial\bar{\gamma}} \right)^{1/3}. \quad (142)$$

The background rate of pair creation is given by eq. (120), namely $e\dot{n}_\pm \sim (c/2)d\rho_{\text{GJ}}/dr = (Ac/2R_{\text{NS}})\rho_{\text{GJ}}$. Substituting for k_* into eq. (142), and neglecting the difference between J and $\rho_{\text{GJ}}c$, one finds

$$\bar{\gamma} > \left(\frac{1}{10^2 A} \frac{\omega_P R_{\text{NS}}}{c} \right)^{2/7} \left(\frac{\partial\ln\dot{n}_\pm}{\partial\ln\bar{\gamma}} \right)^{-2/7} = 20A^{-2/7} B_{\text{NS},14}^{1/7} R_{\text{NS},6}^{1/7} \left(\frac{P}{6\text{ s}} \right)^{-1/7} \left(\frac{\partial\ln\dot{n}_\pm}{\partial\ln\bar{\gamma}} \right)^{-2/7}. \quad (143)$$

The screening of the growing potential perturbation requires that both conditions (138) and (143) be satisfied. The second condition is generally satisfied by our circuit model. The first condition is easily satisfied if $B_{\text{NS}} > 4B_{\text{Q}}$, so that pair creation follows resonant scattering; but it is not satisfied if $B < 4B_{\text{Q}}$. Then the two-stream instability in the pair plasma will be effectively triggered near the neutron star surface, and the non-linear growth of the potential fluctuation into a strong diode may result.

6. DISCUSSION

We now confront the circuit physics described in this paper with a few key observational tests, and then summarize our conclusions. The behavior of the radio magnetars appears to be unusual in several respects in comparison with long-period radio pulsars.

6.1. Application to the Radio Magnetars XTE J1810–197 and 1E 1547.0–5408

6.1.1. Radio Luminosity

The spindown of XTE J1810–197 is transiently accelerated (Camilo et al. 2007a). The polar magnetic field that is deduced from the standard magnetic dipole formula has decreased from $B_{\text{pole}} = 2B_{\text{MDR}} \sim 5 \times 10^{14}$ G to 3×10^{14} G, and a further decrease is possible. The polar field of 1E 1547.0–5408 is inferred to be $B_{\text{pole}} \sim 2 \times 10^{14}$ G. As a result, the actual polar fields of these neutron stars could be weaker than $4B_{\text{Q}}$, in which case the gap model described in §3 is relevant. We first consider whether the power dissipated in the gap can supply the observed radio output.

When the detected pulsed radio emission of XTE J1810–197 was at its peak, the Goldreich-Julian charge flow on the open field lines was $I_{\text{GJ}}/e \simeq B_{\text{MDR}} R_{\text{NS}}^3 \Omega^2 / ec = 2 \times 10^{31} \text{ s}^{-1}$. The mean energy per outflowing particle crossing the gap is $e\Phi_{\text{gap}} = \gamma_{\text{max}} m_e c^2 \sim 5 \times 10^{-3} \text{ erg}$ (eq. [52]), including a factor ~ 0.5 reduction in the gap voltage due to the screening effects of secondary modes of pair creation at a temperature $k_{\text{B}} T_{\text{bb}} \sim 0.25 \text{ keV}$ (Fig. 10). The net dissipated power is therefore $I_{\text{GJ}} \Phi_{\text{gap}} = 1 \times 10^{29} \text{ ergs s}^{-1}$. The peak isotropic output at 40 GHz is, by contrast $4\pi D^2 \nu S_\nu = 1 \times 10^{30} \text{ ergs s}^{-1}$ at $\nu = 100 \text{ GHz}$ at a distance $D = 3 \text{ kpc}$ (Camilo et al. 2007a). The apparent radio output could be enhanced by an order of magnitude by the effects of beaming, but even in that case the two results are barely consistent.

We must therefore consider two alternative possibilities: that the same gap-like structure can form on a broader bundle of magnetic field lines, extending into the closed magnetosphere; or that the power dissipated on the open field lines is much higher than is implied by the gap model of §3. It should be kept in mind that the spindown power of XTE J1810–197 was at least $2.4 \times 10^{33} I_{\text{NS},45} \text{ ergs s}^{-1}$ at its peak, and so it can easily accommodate the radio and infrared output ($L_{\text{IR}} \simeq 1 \times 10^{31} \text{ ergs s}^{-1}$; Rea et al. 2004; Wang et al. 2007).

6.1.2. Peak Emission Frequency and Pulse Width

The pulse duty cycle of the two radio magnetars is much larger than would be expected if the radio emission originated close to the star on the open magnetic field lines. We deduce either that the emission zone is close to the light cylinder, or that there is coherent emission from the closed magnetic field lines. In the case of 1E 1547.0–5408, this effect could be partly explained by a nearly alignment of the magnetic axis with the rotation axis (Camilo et al. 2008). Nonetheless, the fit to the linear polarization curve found by these authors does not require that the tilt angle between $\boldsymbol{\mu}$ and $\boldsymbol{\Omega}$ be nearly as small as $\theta_{\text{open}}(R_{\text{NS}})$, if the radio beam is intrinsically broad. (Indeed, the small a priori probability of detecting a radio beam of angular width $\sim 2\theta_{\text{open}}(R_{\text{NS}})$ from this object can be used to argue that the beam must be broad.)

It is possible to deduce a value of $\gamma\mathcal{M}_\pm$ under the assumptions that i) the radio waves are emitted tangent to the magnetic field lines within a maximum angle which is a multiple N_θ of $\theta_{\text{open}}(r)$; and ii) the emission frequency at radius r is equal to a multiple N_ν of $\nu_{\text{p}\pm}^{\text{rel}}$. We consider an outflowing gas of pairs, within which the plasma frequency is

$$\nu'_{\text{p}\pm} = \frac{\omega'_{\text{p}\pm}}{2\pi} = \left(\frac{2n'_\pm e^2}{\pi m_e} \right)^{1/2} \quad (144)$$

in the bulk frame. The proper density of electrons and positrons is

$$2n'_\pm = \frac{1}{\gamma} (n_{e^+} + n_{e^-}) = \frac{\mathcal{M}_\pm}{\gamma} n_{\text{GJ}} \quad (145)$$

where $\mathcal{M}_\pm \gg 1$ is the number of light charges created per primary Goldreich-Julian charge. We assume for simplicity that the plasma is in bulk motion with a Lorentz factor γ , so that the frequency is increased in the stellar frame by a factor 2γ ,

$$\nu_{P\pm}^{\text{rel}} = \left(\frac{8n_\pm e^2}{\pi m_e} \gamma \right)^{1/2}. \quad (146)$$

The plasma frequency is maximized close to the surface of the star,

$$\begin{aligned} \nu_{P\pm}^{\text{rel}}(R_{\text{NS}}) &= \left[\gamma \mathcal{M}_\pm \frac{2\Omega e B_{\text{NS}}}{\pi^2 m_e c} \right]^{1/2} \\ &= 2.6 \times 10^{12} \left(\frac{\gamma \mathcal{M}_\pm}{10^4} \right)^{1/2} \left(\frac{B_{\text{NS}}}{4B_Q} \right)^{1/2} \left(\frac{P}{6 \text{ s}} \right)^{-1/2} \text{ Hz}. \end{aligned} \quad (147)$$

Outside the maximum radius of pair creation R_\pm , one obtains the usual scaling,

$$\nu_{P\pm}^{\text{rel}}(r) = \left(\frac{r}{R_\pm} \right)^{-3/2} \nu_{P\pm}^{\text{rel}}(R_\pm) \quad (r > R_\pm). \quad (148)$$

Note that $\nu_{P\pm}^{\text{rel}}$ depends on the product $\gamma \mathcal{M}_\pm$, which is approximately invariant if the charges undergo resonant scattering and the scattered photons are able to re-convert to pairs. In the gap model described in §3, one has $\gamma \mathcal{M}_\pm \simeq e\Phi_{\text{gap}}/m_e c^2$.

The tangent to a dipole field lines makes an angle $\frac{3}{2}\theta$ with respect to the magnetic axis when $\theta \ll 1$, and so the pulse duty cycle $\delta t/P$ is given by

$$\frac{\delta t}{P} = \frac{2N_\theta \left(\frac{3}{2}\theta_{\text{open}} \right)}{2\pi} = N_\theta \frac{3\theta_{\text{open}}}{2\pi}. \quad (149)$$

The multiplicity corresponding to a duty cycle $\delta t/P$ at a frequency $\nu = N_\nu \nu_{P\pm}^{\text{rel}}$ is

$$\gamma \mathcal{M}_\pm = \frac{3 \times 10^6}{N_\nu^2 N_\theta^6} \nu_{\text{GHz}}^2 \left(\frac{\delta t/P}{0.1} \right)^6 \left(\frac{P}{6 \text{ s}} \right)^4 \left(\frac{B_{\text{NS}}}{4B_Q} \right)^{-1}. \quad (150)$$

Substituting numbers appropriate to XTE J1810–197 ($\delta t/P = 0.2$ at $\nu = 2$ GHz and $P = 5.44$ s) gives

$$\gamma \mathcal{M}_\pm \sim 5 \times 10^8 N_\nu^{-2} N_\theta^{-6} \quad (\text{XTE J1810–197}). \quad (151)$$

Let us first compare this result with the turbulent flux tube model that is described in Thompson (2008). In that model, the pair multiplicity is $\gamma \mathcal{M}_\pm \sim (eI_{\text{GJ}}/m_e c^3) = 1 \times 10^8$. The plasma frequency at the base of the flux tube then sits in the optical-IR band, and it is possible for the optical-IR emission of XTE J1810–197 to be an upward extension of the spectrum at ~ 100 GHz. If this were the case, a narrower pulse profile would be expected in the IR band as compared with the radio band.

The alternative explanation for the broad pulses and high intensity of the radio emission of XTE J1810–197 is that the outer closed magnetic field lines support a unidirectional discharge. Within a critical angle $\theta(R_{\text{NS}}) \simeq 3^\circ (L_X/10^{34} \text{ ergs s}^{-1})^{-1/2} \simeq 9\theta_{\text{open}}(R_{\text{NS}})$ from the magnetic axis, outflowing relativistic charges are not stopped by resonant scattering of the thermal X-rays. The gap model of §3 gives $\gamma \mathcal{M}_\pm \sim 1 \times 10^4$, which is consistent with eq. (151) if $N_\nu^{1/2} N_\theta \sim 6$. The observed radio power is also reproduced, because the cross-sectional area of the emitting field lines is 30–100 times larger.

Although we cannot in this paper decide between these two possibilities, the spectrum of the radio magnetars provides an important clue. The very high peak frequency of the emission does not, by itself, demand a high plasma density on the open magnetic field lines. But the comparison with ordinary radio pulsars (for which the peak frequency is ~ 0.1 –1 GHz) does suggest that the plasma density is much higher in the radio magnetars than in pulsars, by a factor $> 10^4$ – 10^6 if one uses the scaling $n_\pm \propto \nu_{\text{peak}}^2$.

6.2. Is $4B_Q = 1.8 \times 10^{14} \text{ G}$ a Limiting Polar Magnetic Field for Radio Pulsars?

The distribution of neutron star magnetic fields, as inferred from pulsar spindown, offers important tests of the physics explored in this paper. Considering only sources that are discovered in the radio band,⁹ the distribution of dipole fields has an upper envelope at $B_{\text{MDR}} \simeq 1 \times 10^{14}$ G. The corresponding polar magnetic field is remarkably close to $4B_Q = 1.8 \times 10^{14}$ G. A previous suggestion that radio emission could be quenched in super-QED magnetic fields (Baring & Harding 1998) depends on assumptions about the polarization dependence of photon splitting that are not born out by microphysical calculations (Adler 1971; Usov 2002). Our focus here is different, on the voltage of the open-field circuit and the properties of the gap that may form there.

When the surface magnetic field is stronger than $4B_Q$, the open-field voltage depends on whether a gap is able to form displaced from the surface of the star. The most plausible mechanism of gap formation involves the generation of multiple weak double

⁹ As noted above, the polar fields of the radio magnetars cannot be deduced with precision from their spindown rates due to the presence of large-amplitude torque variations, but are not obviously inconsistent with this bound.

layers in the circuit, seeded by a two-stream instability, which then accumulate into a diode structure with a larger voltage. The two-stream instability is stronger in the low-voltage circuit solution described in §5 than it is the higher-voltage solutions with a gap, but the absence of a sharp boundary at the surface $B = 4B_Q$ may impede the second stage of the process.

Whether or not a gap does form in this situation, pairs are easily created by resonant scattering throughout the inner circuit. Given that the net difference in circuit voltage between the two solutions is only a factor of 10, the detectability of radio pulsations from quiescent neutron stars with $B_{\text{NS}} > 4B_Q$ and $P \sim 1 - 10$ s is probably a matter of flux sensitivity, rather than the presence or absence of emission.

6.3. Summary

1. – We have described a self-consistent circuit solution with a gap at the surface of the neutron star, which requires a current density $|J| > \rho_{\text{GJ}}c$ and a surface magnetic field $B_{\text{NS}} < 4B_Q$. The voltage across the gap is $e|\Phi_{\text{gap}}| \sim 10^4 m_e c^2$ when $k_B T_{\text{bb}} \lesssim 0.15 - 0.2$ keV. We have reconsidered the effects of magnetic field line curvature on the voltage, and find that the octopole component makes the largest contribution to linear order, with the quadrupole contributing to second order, when these two components are treated as a perturbation to the dipole. It is not known whether the two detected radio magnetars have polar magnetic fields stronger or weaker than the critical value $4B_Q$, after allowing for changes in magnetospheric structure resulting from the injection of currents during periods of X-ray activity.

2. – The dominant pair creation mechanism within the gap is the conversion of resonantly scattered photons off the magnetic field when the blackbody temperature is relatively low, $k_B T_{\text{bb}} \lesssim 0.2$ keV. At higher temperatures, the voltage is reduced by secondary modes of pair creation. Up to a temperature of ~ 0.3 keV, the most important such mechanism involves the non-resonant (Klein-Nishina) scattering of X-rays, followed by direct conversion off the magnetic field. At yet higher temperatures, or in fields weaker than $\sim 10^{14}$ G, collisions between gamma rays and thermal X-rays occur at a higher rate. The net effect is to reduce the gap voltage by a factor ~ 0.1 when $k_B T_{\text{bb}} \sim 0.3$ keV.

3. – Screening of the electric field outside the gap can be effected by the polarization of the outflowing pairs. The pairs injected near the outer boundary of the gap continue to downscatter off the ambient thermal X-rays, thereby creating secondary pairs. We have deduced the spectrum of energies that result. Inside a distance $r \sim 10R_{\text{NS}}$, the outflowing pair cloud maintains a charge density equal to ρ_{GJ} , as charges of the opposite sign reverse direction and return to the star. Mildly relativistic electrons and positrons feel a strong drag force near $r \sim 10R_{\text{NS}}$, but a steady, charge-balanced flow remains possible in which the ‘negative’ charges flow outward sub-relativistically.

4. – Where $B > 4B_Q$, the open-field circuit sustains a much lower voltage, because resonantly scattered photons convert directly to free pairs. In the temperature range $k_B T_{\text{bb}} \sim 0.1 - 0.5$ keV, the voltage is reduced by a factor $\sim 0.05 - 0.1$ ($B_{\text{NS}}/4B_Q$) as compared with the gap model evaluated at the threshold field $B_{\text{NS}} = 4B_Q$. We have also derived the voltage distribution through the inner circuit in the case where pair creation is smoothly distributed, at just the rate that is needed to compensate the gradient in ρ_{GJ} . There may be a connection between the quenching of a surface gap at $B_{\text{NS}} > 4B_Q$ and the absence of radio pulsars with dipole fields stronger than 10^{14} G.

5. – The radio output of XTE J1810–197 and 1E 1547.0–5408 is somewhat brighter than is allowed by the gap model of §3, if the emission is restricted to the open dipolar field lines. The radio pulses are also much broader than is typical of long-period radio pulsars (Camilo et al. 2006, 2007b). The same gap model predicts much narrower pulses than are observed if the radio emission frequency is close to the local plasma frequency, and the emission comes from the open magnetic field lines. When combined with the very hard radio spectra, this suggests that the rate of pair creation is much higher in the radio magnetars than in more typical radio pulsars. The wide pulses, hard spectra, and rapid variability of the radio magnetars are more consistent with the electrodynamic model described in Thompson (2008), in which a broad spectrum of Alfvénic turbulence is excited by current-driven instabilities in the outer magnetosphere.

6. – Relativistic pairs flowing outward from an X-ray bright magnetar will suffer strong resonant drag beyond a radius $R_{\text{col}} \sim 50(P/6 \text{ s})^{1/3} R_{\text{NS}}$ if the guiding field line is displaced too far from the magnetic axis. At a spin period of 6 seconds, this critical angle is $\sim 10\theta_{\text{open}}$; but if the spin is faster than $\sim 0.4(L_X/10^{34} \text{ ergs s}^{-1})^{3/4}$ s, then most of the secondary pairs on the open field lines will suffer strong drag outside ~ 10 stellar radii. Radio emission from these charges will be suppressed by induced scattering unless they are continuously reaccelerated. There is therefore a bias against detecting pulsed radio emission from neutron stars with moderately fast spins and high X-ray luminosities (e.g. young magnetars).

This work was supported by the NSERC of Canada. It began as an investigation of the radio death line of magnetars, and I am indebted to Andrei Beloborodov for his contribution to those early efforts. In particular, he provided a cogent argument that pair cascades driven by curvature radiation cannot be self-consistently sustained in magnetar magnetospheres. I also thank him for suggesting some simplifications in the presentation of §2.1, and a correction to the calculation of resonant drag in §4.2. Part of this work was carried out during a visit to Cornell University, which I thank for its hospitality.

REFERENCES

- | | |
|---------------------------------------------------------------|-------------------------------------------------------------------|
| Adler, S. L. 1971, <i>Annals of Physics</i> , 67, 599 | Baring, M. G., & Harding, A. K. 1998, <i>ApJ</i> , 507, L55 |
| Arons, J., & Scharlemann, E. T. 1979, <i>ApJ</i> , 231, 854 | Baring, M. G., & Harding, A. K. 2001, <i>ApJ</i> , 547, 929 |
| Asseo, E., & Khechinashvili, D. 2002, <i>MNRAS</i> , 334, 743 | Baring, M. G., & Harding, A. K. 2007, <i>Ap&SS</i> , 308, 109 |

- Barnard, J. J., & Arons, J. 1982, *ApJ*, 254, 713
 Beloborodov, A. M. 2007, *ArXiv e-prints*, 710, arXiv:0710.0920
 Beloborodov, A. M., & Thompson, C. 2007, *ApJ*, 657, 967
 Berestetskii, V.B., Lifshitz, E.M., & Pitaevskii, L.P. 1982, Oxford: Pergamon Press
 Blumenthal, G. R., & Gould, R. J. 1970, *Reviews of Modern Physics*, 42, 237
 Camilo, F., Ransom, S. M., Halpern, J. P., Reynolds, J., Helfand, D. J., Zimmerman, N., & Sarkissian, J. 2006, *Nature*, 442, 892
 Camilo, F., et al. 2007a, *ApJ*, 663, 497
 Camilo, F., Ransom, S. M., Halpern, J. P., & Reynolds, J. 2007b, *ApJ*, 666, L93
 Camilo, F., Reynolds, J., Johnston, S., Halpern, J. P., & Ransom, S. M. 2008, *ArXiv e-prints*, 802, arXiv:0802.0494
 Cheng, A. F., & Ruderman, M. A. 1977, *ApJ*, 214, 598
 Daugherty, J. K., & Ventura, J. 1978, *Phys. Rev. D*, 18, 1053
 Daugherty, J. K., & Harding, A. K. 1989, *ApJ*, 336, 861
 Dermer, C. D. 1990, *ApJ*, 360, 197
 Dieckmann, M. E. 2005, *Physical Review Letters*, 94, 155001
 Dieckmann, M. E., Shukla, P. K., & Eliasson, B. 2006, *New Journal of Physics*, 8, 225
 Goldreich, P., & Julian, W. H. 1969, *ApJ*, 157, 869
 Gonthier, P. L., Harding, A. K., Baring, M. G., Costello, R. M., & Mercer, C. L. 2000, *ApJ*, 540, 907
 Halpern, J. P., Gotthelf, E. V., Becker, R. H., Helfand, D. J., & White, R. L. 2005, *ApJ*, 632, L29
 Hibsman, J. A., & Arons, J. 2001a, *ApJ*, 554, 624
 Hibsman, J. A., & Arons, J. 2001b, *ApJ*, 560, 871
 Ibrahim, A. I., et al. 2001, *ApJ*, 558, 237
 Kardashev, N. S., Mitrofanov, N. S., & Novikov, I. D. 1984, *AZh*, 61, 1113
 Kuiper, L., Hermsen, W., & Mendez, M. 2004, *ApJ*, 613, 1173
 Kuiper, L., Hermsen, W., den Hartog, P. R., & Collmar, W. 2006, *ApJ*, 645, 556
 Lyubarskii, Y. E., & Petrova, S. A. 1998, *A&A*, 337, 433
 Lyutikov, M., & Thompson, C. 2005, *ApJ*, 634, 1223
 Medin, Z., & Lai, D. 2007, *MNRAS*, 1065
 Mereghetti, S., Götz, D., Mirabel, I. F., & Hurley, K. 2005, *A&A*, 433, L9
 Mestel, L., Robertson, J. A., Wang, Y.-M., & Westfold, K. C. 1985, *MNRAS*, 217, 443
 Muslimov, A. G., & Tsygan, A. I. 1992, *MNRAS*, 255, 61
 Rea, N., et al. 2004, *A&A*, 425, L5
 Ruderman, M. A., & Sutherland, P. G. 1975, *ApJ*, 196, 51
 Scharlemann, E. T., Arons, J., & Fawley, W. M. 1978, *ApJ*, 222, 297
 Shibata, S. 1997, *MNRAS*, 287, 262
 Shibata, S., Miyazaki, J., & Takahara, F. 1998, *MNRAS*, 295, L53
 Shibata, S., Miyazaki, J., & Takahara, F. 2002, *MNRAS*, 336, 233
 Silantev, N. A., & Iakovlev, D. G. 1980, *Ap&SS*, 71, 45
 Sturmer, S. J. 1995, *ApJ*, 446, 292
 Sturrock, P. A. 1971, *ApJ*, 164, 529
 Thompson, C., *ApJ*, submitted (arXiv:0802:2571)
 Thompson, C., & Blaes, O. 1998, *Phys. Rev. D*, 57, 3219
 Thompson, C., Duncan, R. C., Woods, P. M., Kouveliotou, C., Finger, M. H., & van Paradijs, J. 2000, *ApJ*, 543, 340
 Thompson, C., & Duncan, R. C. 2001, *ApJ*, 561, 980
 Thompson, C., Lyutikov, M., & Kulkarni, S. R. 2002, *ApJ*, 574, 332
 Thompson, C., & Beloborodov, A. M. 2005, *ApJ*, 635, 565
 Usov, V. V. 2002, *ApJ*, 572, L87
 Usov, V. V., & Melrose, D. B. 1996, *ApJ*, 464, 306
 Wang, Z., Kaspi, V. M., & Higdon, S. J. U. 2007, *ApJ*, 665, 1292
 Woods, P. M., Kouveliotou, C., Göğüş, E., Finger, M. H., Swank, J., Markwardt, C. B., Hurley, K., & van der Klis, M. 2002, *ApJ*, 576, 381
 Woods, P. M., & Thompson, C. 2006, in *Compact Stellar X-ray Sources*, eds. W. H. G. Lewin and M. van der Klis (Cambridge: Cambridge University Press) 547
 Zhang, B., & Harding, A. K. 2000, *ApJ*, 535, L51
 Zhang, B., & Qiao, G. J. 1998, *A&A*, 338, 62

APPENDIX

SOURCES OF GRADIENT IN COROTATION CHARGE DENSITY

The voltage on the open magnetic field lines is dominated by the gradient in the corotation charge density in the case where the first order difference between J and $\rho_{GJ}c$ is compensated by a returning flow of charges of the sign opposite to the local corotation charge. Here we compare the effect of general relativistic frame dragging (Muslimov & Tsygan 1992) with field line curvature as dominated by a quadrupolar and octopolar magnetic field.

A purely dipolar magnetic field in a Schwarzschild spacetime has the shape

$$\mathbf{B}(r) = \frac{f(r)}{f(R_{NS})} \mathbf{B}_{\text{dipole}}(r), \quad (\text{A1})$$

where $f(r) = 1 + \sum_{k=0}^{\infty} \frac{3}{k+3} (2GM_{NS}/c^2 r)^k$ (Muslimov & Tsygan 1992, eq. 32). The prefactor here describes the deviation of the poloidal magnetic field lines from the shape they would have in the absence of gravity. It does not affect the voltage directly, because both the charged particle flux and the magnetic flux satisfy the same conservation equation. The relativistic charge density $\alpha(r)\rho_{GJ}(r)$ has the form (5), taking into account the effects of frame dragging. When evaluating the lapse function, the stellar rotation can be neglected: on has

$$\alpha(r) = \left(1 - \frac{2GM_{NS}}{c^2 r}\right)^{1/2} \quad (\text{A2})$$

outside the star. It is sufficient to take $\alpha \rightarrow 1$ and $f \rightarrow 1$ in all expressions, because the magnetic flux density and the relativistic current density $\mathbf{J} = \alpha\rho\mathbf{v}$ and the magnetic flux density satisfy the same conservation law¹⁰ $\nabla \cdot \mathbf{B} = \nabla \cdot \mathbf{J} = 0$.

An additional mechanism for voltage generation becomes significant for a more general magnetic configuration in which the open field lines are strongly curved. The ratio ρ_{GJ}/B increases with distance from the star on those field lines that bend toward the spin axis. In the absence of pair creation this implies an increasing mismatch $|\rho| > |\rho_{GJ,0}|$, and a voltage is generated that accelerates the Goldreich-Julian flow (e.g. Barnard & Arons 1982; Asseo & Khechinashvili 2002). This effect dominates over the frame-dragging effect beyond a certain radius, and can be especially important in magnetars due to the screening of the parallel electric field by direct pair creation close to the star.

We focus here on the case where the magnetic field is predominantly dipolar beyond zone I. The presence of a higher multipole (quadrupole or octopole) causes a bending of the open dipolar field lines. The angular deflection $\delta\theta(r)$ can be deduced by working inward from the light cylinder. The radial component of the magnetic field is dominated by the dipole component, $B_D = B_{NS}(r/R_{NS})^{-3}$. Well inside the light cylinder, but still far from the magnetar surface, the non-radial field component on the

¹⁰ Here ∇ is the gradient operator in Minkowski space.

open-flux bundle is dominated by the higher multipole, e.g.,

$$B_\theta(r) \simeq B_\ell(R_{\text{NS}}) \left(\frac{r}{R_{\text{NS}}}\right)^{-\ell-2} \equiv \varepsilon_\ell B_{\text{NS}} \left(\frac{r}{R_{\text{NS}}}\right)^{-\ell-2}. \quad (\text{A3})$$

We suppose that this additional multipole is oriented randomly with respect to the magnetic dipole axis. Then

$$\delta\theta(r) \simeq \int_r^\infty \frac{B_\theta(r)}{B_D(r)} \frac{dr}{r} = \frac{\varepsilon_\ell}{\ell-1} \left(\frac{r}{R_{\text{NS}}}\right)^{-\ell+1}. \quad (\text{A4})$$

The parameter ε_ℓ contains the angular dependence of the ℓ -pole.

The lowest-order multipole component which makes a significant contribution to voltage and curvature of the open field lines is the octopole.¹¹ To see this, note that the transverse deflection of the open magnetic flux bundle away from a pure dipole is $L_\perp = r\delta\theta(r) \propto r^{2-\ell}$, which is constant for a quadrupole. More generally the curvature radius can be found from

$$R_C^{-1} = |(\hat{B} \cdot \nabla)\hat{B}|, \quad (\text{A5})$$

which in combination with

$$\hat{B} \simeq [1 - b_\theta(r)^2]^{1/2} \hat{r} + b_\theta(r) \hat{\theta}; \quad b_\theta(r) \equiv \frac{B_\ell(r)}{B_D(r)} \quad (\text{A6})$$

gives

$$R_C^{-1} = \frac{1}{r} \left| \left(\frac{\partial(rb_\theta)}{\partial r} + b_\theta \frac{\partial b_\theta}{\partial \theta} \right) \hat{\theta} - b_\theta \frac{\partial(rb_\theta)}{\partial r} \hat{r} \right|. \quad (\text{A7})$$

to second order in b_θ . A single additional multipole imparts a curvature radius

$$R_C = \frac{r}{(\ell-2)(\ell-1)\delta\theta(r)} = \frac{R_{\text{NS}}}{(\ell-2)\varepsilon_\ell} \left(\frac{r}{R_{\text{NS}}}\right)^\ell, \quad (\text{A8})$$

to lowest order in b_θ . This expression gives infinite R_C for $\ell = 2$, and

$$R_C = \frac{r}{2\delta\theta} = \left(\varepsilon_2 \frac{\partial \varepsilon_2}{\partial \theta} + \varepsilon_3 \right)^{-1} \left(\frac{r}{R_{\text{NS}}}\right)^3 R_{\text{NS}} \quad (\text{A9})$$

when an octopole is added to the dipole. The quadrupole provides a second-order correction to the octopole curvature, which has the same scaling in radius, and is of comparable magnitude if $\varepsilon_3 \sim \varepsilon_2^2$.

When the magnetic field is mainly dipolar, the opening angle is given approximately by the dipole formula,

$$\begin{aligned} \theta_{\text{open}}(r) &= \left[f_{\text{open}}(\chi) \frac{\Omega r}{c} \right]^{1/2} \\ &= 0.014 f_{\text{open}}^{1/2} R_{\text{NS},6}^{1/2} \left(\frac{P}{\text{s}}\right)^{-1/2} \left(\frac{r}{R_{\text{NS}}}\right)^{1/2} \text{ rad.} \end{aligned} \quad (\text{A10})$$

The factor $f_{\text{open}}(\chi) = O(1)$ corrects for an inclination angle $\chi \neq 0$ between the magnetic moment and the rotation axis; we generally set $f_{\text{open}} = 1$ in expressions in this paper. The tilt of the field lines with respect to the magnetic dipole axis can easily be much larger than θ_{open} . For example, a quadrupole/octopole component of magnitude

$$\tilde{\varepsilon}_3 \equiv \varepsilon_3 + \varepsilon_2 \frac{\partial \varepsilon_2}{\partial \theta} > 0.012 f_{\text{open}}^{1/2} R_{\text{NS},6}^{1/2} \left(\frac{P}{\text{s}}\right)^{-1/2} \left(\frac{r}{R_{\text{NS}}}\right)^{1/2} \quad (\text{A11})$$

is sufficient to impart a tilt $\delta\theta > \theta_{\text{open}}$ at a radius r . In this situation, both $\delta\theta$ and ρ_{GJ} are approximately constant across the open flux bundle.

The electrostatic potential, as given by eq. (A18), depends on the deviation of the charge density from the local corotation density.¹² In this case, there is a direct relation between the curvature of the open flux bundle and the gradient in ρ_{GJ} parallel to the magnetic field. One has

$$\frac{d(\rho_{\text{GJ}}/B)}{dl} = \frac{\Omega}{2\pi c} \cdot [(\hat{B} \cdot \nabla)\hat{B}] = \frac{\Omega}{2\pi c R_C} \sin \chi \cos \phi_C, \quad (\text{A12})$$

¹¹ To linear order in the multipole amplitude. This conclusion presupposes the dominance of the dipole component of the magnetic field in the acceleration zone. If the dipole component were absent, then a quadrupole by itself would still not supply significant field line curvature. The opening angle in that case would be $\theta_{\text{open}} \sim \Omega r/c$, and the curvature radius would be comparable to the light cylinder radius, $R_C \sim r/\theta_{\text{open}} \sim c/\Omega$. A mixture of multipoles is required to provide an effective particle accelerator.

¹² For simplicity we set the lapse function $\alpha \rightarrow 1$ in what follows.

or, equivalently,

$$B \frac{d(\rho_{\text{GJ}}/B)}{dr} = \frac{\rho_{\text{GJ}}}{R_C} \sin \chi \cos \phi_C. \quad (\text{A13})$$

We have made use of the fact that $(\hat{B} \cdot \nabla)\hat{B}$ points in the θ -direction in the plane of curvature of the open magnetic field lines.¹³ Here ϕ_C is the angle by which the plane of curvature is rotated with respect to the $\mu - \Omega$ plane. The zero of ϕ_C is defined so that the field lines bend *toward* the rotation axis when $\cos \phi_C > 0$. There is no acceleration when $\cos \phi_C < 0$.

Limiting Voltage on a Slender Magnetic Flux Tube.

For completeness, we examine the voltage in an extended gap which has a length Δr much larger than the radius $\theta_{\text{open}} r$ of the open magnetic field bundle. When the star rotates steadily and the magnetic field is fixed in the corotating frame, an electrostatic potential $\Phi(r)$ can be introduced, which satisfies the equation,

$$\nabla \cdot (\alpha^{-1} \nabla \Phi) = -4\pi(\rho - \rho_{\text{GJ}}). \quad (\text{A14})$$

Then the electric field component along \mathbf{B} is given by

$$E_{\parallel} = \alpha^{-1} \hat{B} \cdot \nabla \Phi. \quad (\text{A15})$$

Once again, we make the approximation $\alpha \rightarrow 1$. We approximate the open flux bundle as being locally cylindrical, with a cross-sectional area

$$S_{\perp} \simeq \pi \theta_{\text{open}}^2 r^2. \quad (\text{A16})$$

Choosing a longitudinal coordinate r and transverse (cylindrical) radius $\varpi = \theta r$, Gauss' law can be expressed as

$$\frac{1}{\varpi} \frac{\partial}{\partial \varpi} \left[\varpi \frac{\partial \Phi}{\partial \varpi} \right] + \frac{d^2 \Phi}{dr^2} = -4\pi(\rho - \rho_{\text{GJ}}). \quad (\text{A17})$$

It is usual to apply the boundary condition $\Phi = 0$ at $\varpi = \theta_{\text{open}} r$, which must however be reconsidered when the closed magnetic field lines are twisted by the release of internal stresses. In this situation, a modest voltage $\sim 10^2 - 10^3$ V develops on the closed field lines, as is required to sustain the current (Beloborodov & Thompson 2007). The power dissipated in the closed-field circuit is drawn from the energy of the toroidal magnetic field, and the gradual relaxation of this twist is associated with a time derivative of the longitudinal component of the vector potential. The twist on the open magnetic field lines is, by contrast, continually replenished by the rotation of the star, and decreases only adiabatically as the star spins down. We therefore retain the boundary condition $\Phi = 0$ at $\varpi = \theta_{\text{open}} r$, but it should be understood that this boundary condition could be modified if the outer magnetosphere were subject to fast, current-driven instabilities.

A simple solution to eq. (A17) is obtained by neglecting the longitudinal component of the laplacian and taking both ρ and ρ_{GJ} to be constant across the open flux bundle. This approximation is reasonably accurate outside a distance $r - R_{\text{NS}} \sim (\theta_{\text{open}}/2)R_{\text{NS}}$ from the neutron star surface. The solution is

$$\Phi(r, \theta) = \frac{I_{\text{GJ}}}{c} \left(\frac{\rho}{\rho_{\text{GJ}}} - 1 \right) \left(1 - \frac{\theta^2}{\theta_{\text{open}}^2} \right). \quad (\text{A18})$$

Here

$$I_{\text{GJ}}(r) = S_{\perp}(r) \alpha(r) \rho_{\text{GJ}}(r) c \quad (\text{A19})$$

is the net current along the open field-line bundle. The twist on the open magnetic field lines is supported by the outward flow of the corotation charge. Neglecting the effect of frame dragging, the charge flow rate is given by

$$\frac{|I_{\text{GJ}}^0|}{e} = \frac{\Omega^2 B_{\text{NS}} R_{\text{NS}}^3}{2ec} = 4 \times 10^{31} B_{\text{NS},15} R_{\text{NS},6}^3 \left(\frac{P}{6 \text{ s}} \right)^{-2} \text{ s}^{-1}. \quad (\text{A20})$$

An important feature of eq. (A18) is the reversal in sign compared with the solution that would be obtained by neglecting the transverse component of the laplacian in favor of the longitudinal component, and applying the boundary condition $\Phi(R_{\text{NS}}, \theta) = 0$. This means that if the charge density ρ decreases with radius more rapidly than ρ_{GJ} , then an electric field is generated that is of the right sign to drive the charges away from the star (Scharlemann et al. 1978; Muslimov & Tsygan 1992).

We suppose that screening is absent beyond some radius R_* . Enough charges are created inside this radius so that $\rho = \rho_{\text{GJ}}$; but that the charge density is determined by the continuity of the outward charge flow farther out in the magnetosphere. The voltage solution beyond this radius is, then

$$\Phi(r, \theta) = \kappa_* \frac{I_{\text{GJ}}^0}{c} \left[\left(\frac{r}{R_*} \right)^{-3} - 1 \right] \left(1 - \frac{\theta^2}{\theta_{\text{open}}^2} \right). \quad (\text{A21})$$

Here we have used

$$\kappa_* \equiv \kappa(R_*) = \frac{2GI_{\text{NS}}}{R_*^3 c^2}. \quad (\text{A22})$$

¹³ To leading order in the quadrupole/octopole amplitudes; eq. [A7].

Expanding equation (A21) near R_* gives

$$\Phi(R_* + \Delta r) - \Phi(R_*) \simeq -3\kappa_* \frac{I_{\text{GJ}}^0}{c} \left(\frac{\Delta r}{R_*} \right). \quad (\text{A23})$$

The limiting Lorentz factor of an electron (or positron, if $\rho_{\text{GJ}} > 0$) flowing beyond $r = R_*$ is

$$\begin{aligned} \gamma_{\text{max}}(R_*) &= \frac{e[\Phi(r \gg R_*) - \Phi(R_*)]}{m_e c^2} = \kappa(R_*) \frac{e I_{\text{GJ}}^0}{m_e c^3} \\ &= \frac{G I_{\text{NS}} \Omega^2 e B(R_*)}{m_e c^6} = 5.3 \times 10^7 I_{\text{NS},45} \left[\frac{B(R_*)}{10^{15} \text{ G}} \right] \left(\frac{P}{6 \text{ s}} \right)^{-2}. \end{aligned} \quad (\text{A24})$$

Now let us turn to the case where the gradient in ρ_{GJ} is dominated the quadrupole and octopole magnetic field. The voltage that develops in the absence of screening can be obtained by integrating eq. (A12) along \mathbf{B} ,

$$\Phi(r) = \kappa_\ell \frac{\Omega^2 \mu}{(\ell-1)c^2} \left(\frac{R_*}{R_{\text{NS}}} \right)^{-\ell+1} \left[1 - \left(\frac{r}{R_*} \right)^{-\ell+1} \right] \quad r > R_*, \quad \ell \geq 3. \quad (\text{A25})$$

In this expression, $\mu = \frac{1}{2} B_{\text{NS}} R_{\text{NS}}^3$ is the magnetic moment of the star, and

$$\kappa_\ell \equiv (\ell-2)\varepsilon_\ell \sin \chi \cos \phi_C. \quad (\text{A26})$$

The expansion near $r = R_*$ is given by

$$\Phi(R_* + \Delta r) - \Phi(R_*) \simeq \kappa_\ell \frac{I_{\text{GJ}}^0}{c} \left(\frac{R_*}{R_{\text{NS}}} \right)^{-\ell+1} \left(\frac{\Delta r}{R_*} \right). \quad (\text{A27})$$

The limiting Lorentz factor of accelerated electrons (or positrons, if $\rho_{\text{GJ}} > 0$) that can be accelerated outside a radius R_* is

$$\gamma_{\text{max}}(R_*) = \frac{\kappa_\ell}{\ell-1} \frac{e I_{\text{GJ}}^0}{m_e c^3} \left(\frac{R_*}{R_{\text{NS}}} \right)^{-\ell+1}. \quad (\text{A28})$$

We can now compare the voltages that are induced by the frame dragging and field-line curvature effects. Outside a radius $R_* > R_{\text{NS}}$, one has

$$\frac{\Phi(\text{field curvature})}{\Phi(\text{frame dragging})} = \frac{\kappa_\ell}{(\ell-1)\kappa(R_{\text{NS}})} \left(\frac{R_*}{R_{\text{NS}}} \right)^{-\ell+4} = 6.7 \frac{\kappa_\ell}{\ell-1} \frac{R_{\text{NS},6}^3}{I_{\text{NS},45}} \left(\frac{R_*}{R_{\text{NS}}} \right)^{-\ell+4}. \quad (\text{A29})$$

In the case where quadrupole/octopole components are present, one can define an effective octopole amplitude

$$\tilde{\kappa}_3 = \left(\varepsilon_3 + \varepsilon_2 \frac{\partial \varepsilon_2}{\partial \theta} \right) \sin \chi \cos \phi_C, \quad (\text{A30})$$

following eq. (A9). One then has

$$\frac{\Phi(\text{field curvature})}{\Phi(\text{frame dragging})} = 3.4 \tilde{\kappa}_3 \frac{R_{\text{NS},6}^3}{I_{\text{NS},45}} \left(\frac{R_*}{R_{\text{NS}}} \right). \quad (\text{A31})$$

In the particular case where $B = 4B_Q$, the quadrupole/octopolar components of the magnetic field will dominate the effects of frame dragging if $\tilde{\kappa}_3 > 0.17 B_{\text{NS},15}^{-1/3} I_{\text{NS},45} R_{\text{NS},6}^{-3}$.

A deviation of ρ from ρ_{GJ} also arises due to the flaring of the dipolar field lines, even in the absence of higher multipoles in the magnetic field (Scharlemann et al. 1978). This third effect is less important¹⁴ than frame dragging if $d(B_\theta/B_r)d \ln r \simeq \theta_{\text{open}}/4 \ll 3\kappa$. This inequality translates into an upper bound on the surface polar magnetic field,

$$B_{\text{NS}} < 1.3 \times 10^{16} \left(\frac{P}{6 \text{ s}} \right)^{3/7} \text{ G}. \quad (\text{A32})$$

The dipole fields of all magnetars easily satisfy this inequality.

¹⁴ We consider the simplest case of an aligned rotator in making this estimate.